**Smart Structures and Systems**, *Vol. 27, No. 4 (2021) 571-592*
DOI: https://doi.org/10.12989/sss.2021.27.4.571


# Nonlinear analysis of concrete-filled single and double skin steel tubular tapered columns under axial loading

Süleyman İpek*[1] and Esra Mete Güneyisi [2a]

[1] *Department of Architecture, Bingöl University, 12000, Bingöl, Turkey*
[2] *Department of Civil Engineering, Gaziantep University, 27310, Gaziantep, Turkey*

(*Received January 20, 2020, Revised December 22, 2020, Accepted December 31, 2020*)

**Abstract.** In this study, the structural response of concrete-filled single and double skin steel tubular (CFST and CFDST) composite tapered columns was investigated through the finite element method (FEM). In the development of the FEM model, the concentric axial loading condition and circular section were adopted. Experimental results available in the literature were used to verify the proposed FEM model. In addition, a parametric study was performed to visualize the effectiveness of tapered angle and material strengths on the ultimate capacity of CFST and CFDST tapered columns. To this aim, a total of 60 tapered column samples (including 30 CFST and 30 CFDST columns) were modeled by taking into consideration five tapered angles, two steel tube yield strengths, and three concrete cube compressive strengths. The verification of the FEM model revealed that the developed model has a reliable and trustable assessment capability. It was noticed that the tapered angle was the most crucial parameter, influencing significantly the ultimate axial strength and stiffness of both CFST and CFDST composite tapered columns. As well, it was overtly beheld from the study that CFST composite tapered column specimens had better ultimate axial strength values than CFDST composite tapered column specimens with the same sectional and material properties.

**Keywords:** concrete-filled steel tube; concrete-filled double skin tube; finite element method; modeling; tapered column

## 1. Introduction

Steel tubular members with circular, square, or rectangular hollow cross-sections have been used for a long period and applied widely in the structures. These members have been preferred due to the effective production process and advance in improved connection details. Similar to the other types of structural members, the following issues such as the member capacity in tension or compression, rotation and flexural ultimate capacity of the cross-sections, strength limited by buckling of the sections, connection design and, if required, fatigue properties needs to be considered in their design (Kulak 1996, D'Aniello *et al*. 2014, 2015). Even though the steel tubular sections alone are satisfactorily utilized, in recent years, composite members in which steel tubular sections together with concrete take substantial attention.

The composite tubular columns, which are achieved by using favorable properties of steel and concrete to manufacture a new element that carries superior characteristics of both steel and concrete, are considered as one of the most significant structural elements. The most widely used composite column is the reinforced concrete columns in which the reinforcing steel bars are encompassed by the concrete to resist both tensile and compressive loads. In case of high load carrying capacity and/or high earthquake resistance of the columns are required; the concrete-encased steel columns can be preferable. This type of column consists of concrete or reinforced concrete that surrounds the H-shaped steel member. Concrete-filled steel tubular (CFST) column is a precious composite column type. These types of composite columns comprise the steel tube and concrete infill and they perform high strength and good deformation capability (Chen *et al*. 2018, Ding *et al*. 2017, Uenaka *et al*. 2010, Zhang *et al*. 2016). As well, the concrete-filled double skin steel tubular (CFDST) columns, which are a new species of CFST columns, could also be regarded as composite columns (Zhao and Han 2006). The inner steel tube distinguishes the CFDST columns from the CFST columns. While the steel tube and concrete infill are involved in the CFST columns as delineated in Fig. 1(a), the CFDST columns consist of two centrally placed steel tubes (known as outer and inner steel tubes) with concrete-filled between them (known as concrete annulus) as delineated in Fig. 1(b). Both CFST and CFDST columns have significant advantages of being quickly constructed and economical. At first, the context of double skin composite was proffered to be used in submerged tube tunnels (Tomlinson *et al*. 1989) and then further studies engendered new possible utilization areas for double skin composites such as nuclear containment, blast-resistant shelters, and liquid and gas retaining structures (Wright *et al*. 1991a, b). Recently, a multitude of studies exploring the possibility to be applied on the constructional purposes have been conducted on the CFDST columns (Han *et al*. 2004, Kim *et al*. 2013, Lin and

*Corresponding author, Ph.D., Assistant Professor, E-mail: sipek@bingol.edu.tr
[a] Ph.D., Professor, E-mail: eguneyisi@gantep.edu.tr



ISSN: 1738-1584 (Print), 1738-1991 (Online)

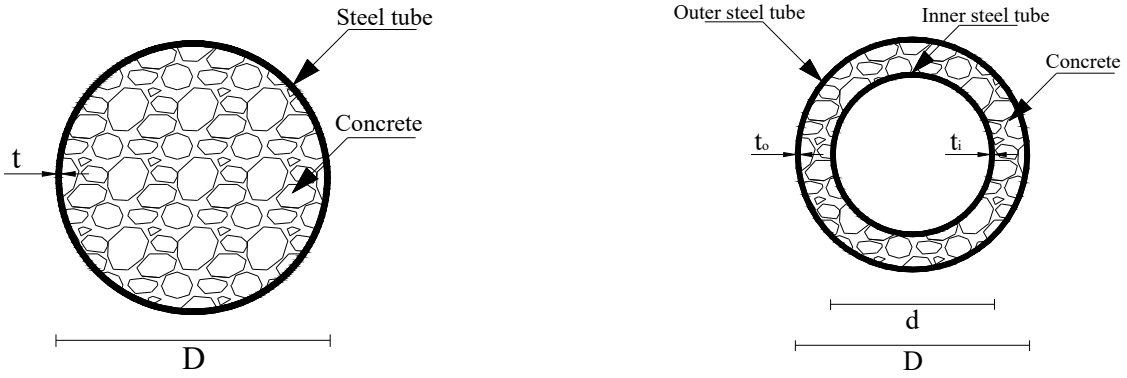


(a) CFST column (b) CFDST column

Fig. 1 Cross-sectional patterns

Tsai 2001, Shekastehband *et al*. 2018, Tao *et al*. 2004, Uenaka *et al*. 2010, Wei *et al*. 1995, Zhao *et al*. 2002a, b, 2010). These researches revealed that the CFDST columns have similar demeanors to CFST columns (Li *et al*. 2012). Also, the hollow section in CFDST columns provides a lower structural weight while maintaining the large energy absorption capacity (Hassan *et al*. 2016, İpek and Güneyisi 2020, Li *et al*. 2012, Uenaka *et al*. 2010).

The concrete-filled single or double skin steel tubular tapered column is a very special kind of composite member having the cross-section diminishing from bottom to top as its height increases. The economical side of these types of columns may be considered as the main advantage and also, they can be utilized in the structures in order to yield the architectural demands (Li *et al*. 2012). Besides, in addition to their aesthetics semblance, they exhibit identical mechanical performances with the members having uniform cross-sections (Li *et al*. 2013). However, the experimental results indicated that since the cross-section size of the members diminishes from bottom to top of the column, they have lower ultimate axial strength than the one having a uniform cross-section.

In the literature, there are limited studies of such columns. For example, Han *et al*. (2010) and Ren *et al*. (2017) studied experimentally on the CFST composite tapered columns and Li *et al*. (2012) and Han *et al*. (2011) presented researches about the CFDST composite tapered columns. The main concern in these studies was to investigate the influence of the tapered angle ($\theta$) on the ultimate axial strength of composite tapered columns. The results of these studies revealed that the performance of both concrete-filled single and double skin steel tubular composite tapered columns decreased when compared with the traditional straight columns (Han *et al*. 2010, 2011, Li *et al*. 2012, Ren *et al*. 2017). Han *et al*. (2010) suggested that this type of column may be used as members, which can resist the vertical loads. Li *et al*. (2012) stated that especially the CFDST tapered columns have been used in the construction of electrical transmission towers and also, it was emphasized that the knowledge about such type of columns are still scarce though they have already been utilized in the practical application. Also, these types of members can be employed in high-rise buildings or industrial structures where the lower columns have sometimes a higher cross-section than the upper columns (Han *et al*. 2010). Moreover, Han *et al*. (2010) attempted to use the existing code formulas in the prediction of ultimate axial strength of CFST composite tapered columns and the research results indicated that the prediction capability of existing code formulas are significantly poor when they are used for the ultimate axial strength assessment of special concrete-filled steel tubular columns.

Due to the lack of information about the attitude of concrete-filled single and double skin steel tubular composite tapered columns in the literature and the poor prediction performance of the existing code formulas regarding the ultimate axial strength, a model that could be useful for simulation and visualization of the characteristics of such type of columns is requisite. For this reason, a new model was developed to simulate and analyze both CFST and CFDST composite tapered columns in this study. The model herein was generated by using the finite element method (FEM) mediated through ABAQUS CAE (2014) software.

The developed model was suggested to be utilized in the prediction of the performance of both concrete-filled single and double skin steel tubular composite tapered columns. During the development of the model, the axially loading condition and circular cross-section for both tapered column types were considered as shown in Figs. 2(a)-(b). The experimental test results existing in the literature were handled to verify the efficacy, accuracy, and reliability of the developed model. Subsequently, to examine the influences of the tapered angle and material strengths on the ultimate axial strength of such types of tapered columns, a parametric study was conducted. 30 CFST composite tapered column samples were modeled by taking into consideration five tapered angles, two steel tube yield strengths, and three concrete cube compressive strengths, and after, the parametric study results were statistically evaluated. Besides, 30 CFDST composite tapered column samples were also modeled having the same sectional and material properties as CFST composite tapered column samples to display the impact of second steel skin that was used as an inner steel tube in the production of the CFDST composite tapered columns. The analysis of the results was given and discussed comparatively.

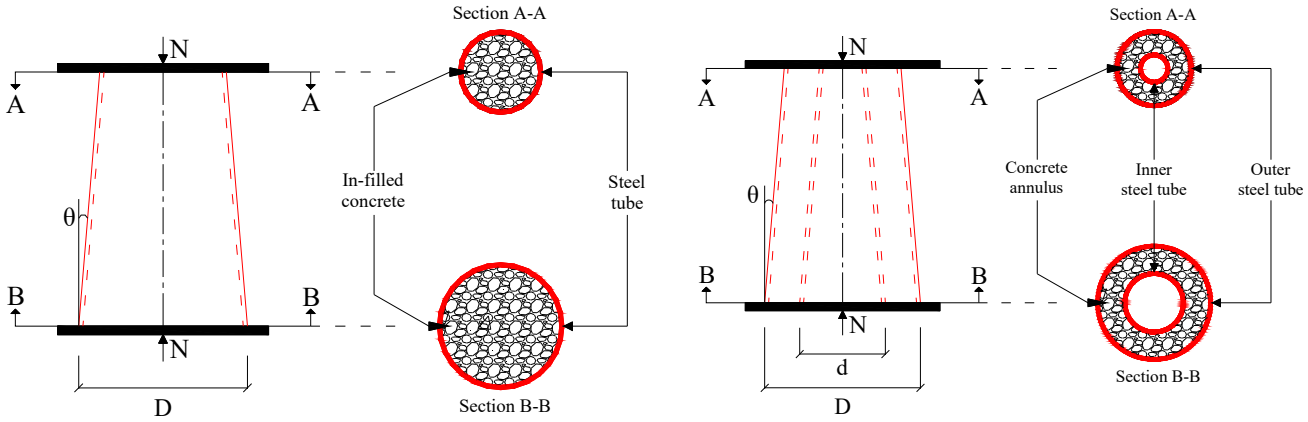


(a) CFST composite tapered column (b) CFDST composite tapered column

Fig. 2 Intricate specimens and test configuration

## 2. FEM model

The finite element program named ABAQUS CAE (2010) was employed to analyze and simulate the nonlinear response of the CFST and CFDST composite tapered columns having a circular section under the axial loading condition. The material definition especially the nonlinear behavior, interaction, surface identification, element type, mesh selection, loading, and boundary condition are elucidated in detail in the following sections.

### *2.1 Material modeling*

Both CFST and CFDST tapered columns compose of steel tubes and concrete infill. In this study, they were modeled as including bottom and top plates. The material definitions used for the steel tube were also utilized for the endplates. The steel and concrete behaviors adopted in the model are given below.

#### *2.1.1 Modeling of steel*

In the literature, there are various stress-strain models, which have been used by many researchers in the modeling of steel such as the elastic-perfectly plastic model (Hu *et al*. 2003, Schneider and Member 1998), the elastic-plastic model with linear hardening (Guo *et al*. 2007, Xiong and Zha 2007) or multi-linear hardening (Han *et al*. 2007).

It was expressed by Tao *et al*. (2013b) that the stress-strain relationship selection has no significant effects on the load-carrying capacity of the member and it was reported that only the load-deformation curve in a later stage of the member is relatively affected by the stress-strain relationship of steel.

The steel material, in this study, was defined by using the elastic-plastic model with strain-hardening that was proposed by Tao *et al*. (2013a) as schematically indicated in Fig. 3. Besides, it was proposed that the model is valid for the yield strength values ranging between 200 and 800 MPa (Tao *et al*. 2013a). The elastic properties of the steel were elucidated in the first region, which starts from the origin and ends at the yield point. The elastic constants such as modulus of elasticity and Poisson's ratio were set in this region. If the elastic modulus and Poisson's ratio are not known or not provided, it can be considered as $200 \times 10^3$ MPa and 0.3, respectively. The second part in the stress versus strain relationship of the steel material was considered as the strain-hardening region and as can be overtly seen from Fig. 3, the yield, plastic, and ultimate strain values, yield and ultimate strength, and elastic modulus of steel are necessary to acquire the stress-strain relation of steel material.

Following expressions as recommended by Tao *et al*. (2013a) were used in the determination of the strain values

$$\varepsilon_y = \frac{f_{sy}}{E_s} \tag{1}$$

$$\varepsilon_p = \begin{cases} 15\varepsilon_y & f_{sy} \le 300\ MPa \\ \left[15 - 0.018\left(f_{sy} - 300\right)\right]\varepsilon_y & 300\ MPa < f_{sy} \le 800\ MPa \end{cases} \tag{2}$$

$$\varepsilon_u = \begin{cases} 100\varepsilon_y & f_{sy} \le 300\ MPa \\ \left[100 - 0.15\left(f_{sy} - 300\right)\right]\varepsilon_y & 300\ MPa < f_{sy} \le 800\ MPa \end{cases} \tag{3}$$

where $\varepsilon_y$, $\varepsilon_p$, and $\varepsilon_u$ are the yield, plastic, and ultimate strain of steel tube, respectively, $f_{sy}$ and $E_s$ are the yield strength and elastic modulus of steel tube, respectively.

Furthermore, Tao *et al*. (2013a) proposed an equation by which the steel ultimate strength can be determined by employing the steel yield strength value as given in the following

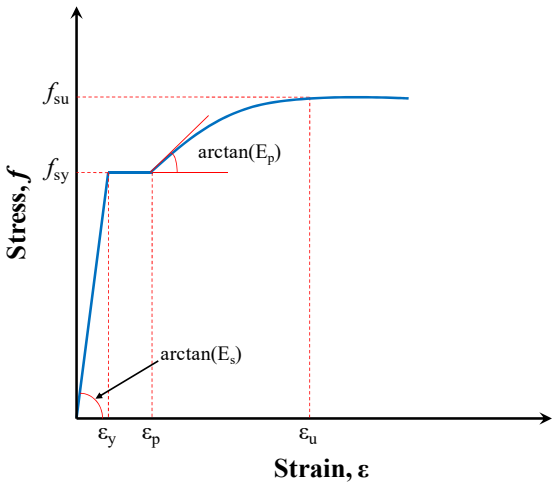


Fig. 3 Stress-strain curve for the steel tubes and end plates (Tao *et al*. 2013a)

study, the model named Concrete Damaged Plasticity (CDP) existing in ABAQUS CAE was adopted to describe the behavior of the concrete utilized as infill material. The plasticity of concrete is defined by the CDP model regarding the unique yield function with the non-associated flow and a Drucker-Prager hyperbolic flow potential function (Huang *et al*. 2010). Namely, isotropic damaged plasticity context combined with isotropic tensile and compressive plasticity is handled by the CDP model in order to reflect the inelastic characteristic of concrete (Hassanein and Kharoob 2014). The plasticity parameters to be determined in this model are the flow potential eccentricity ($e$), viscosity parameter, the ratio of the strength under biaxial compression to the strength under uniaxial compression ($f_{b0}/f_{c0}$), the ratio of the second stress invariant on the tensile meridian to that on the compressive meridian ($K_c$) (Tao *et al*. 2013b), and the dilation angle ($\psi$). These are the main CDP model parameters. In addition to these

$$f_{su} = \begin{cases} \left[1.6 - 2x10^{-3}\left(f_{sy} - 200\right)\right] f_{sy} & 200\ MPa \le f_{sy} \le 400\ MPa \\ \left[1.2 - 3.75x10^{-4}\left(f_{sy} - 400\right)\right] f_{sy} & 400\ MPa < f_{sy} \le 800\ MPa \end{cases} \quad (4)$$

where $f_{su}$ is the steel's ultimate strength.

The nonlinear region of the stress-strain curve of steel material, namely the strain-hardening region, could be calculated by the following expressions that were suggested by Tao *et al*. (2013a)

$$f_s = f_{su} - \left(f_{su} - f_{sy}\right)\left(\frac{\varepsilon_u - \varepsilon_s}{\varepsilon_u - \varepsilon_p}\right)^p \quad (5)$$

where $f_s$ and $\varepsilon_s$ are the stress and strain in the nonlinear region of steel material, respectively, and $p$ is the strain-hardening exponent that can be determined by the expression below

$$p = E_p\left(\frac{\varepsilon_u - \varepsilon_p}{f_{su} - f_{sy}}\right) \quad (6)$$

where $E_p$ is the modulus in the strain-hardening region that was assumed to be equal to 2% of elastic modulus (Tao *et al*. 2013a).

### 2.1.2 Modeling of concrete

Concrete inherently indicates brittle behavior but performs diverse failing mechanisms that can be stated as crushing and cracking in compression and tension, respectively (Huang *et al*. 2010). However, the utilization of concrete in the steel tube as infill material changes its nature. The steel, which envelops the concrete, supply extra strength to concrete and enhances its ductility (Tao *et al*. 2013a). The amount of confinement that is provided by surrounding steel is directly related to its diameter-to-thickness ratio. For this reason, the stress-strain relationship of unconfined concrete cannot be employed to simulate concrete behavior in the model when the diameter-to-thickness ratio of the steel tube is less than 150. In order to achieve accurate and reliable simulation from the model, the behavior of concrete should be well-defined. In this parameters, the strain hardening and softening behavior of concrete under compressive loading and its tensile behavior should also be described in the CDP model. Also, the elastic constants of the concrete such as elastic modulus and Poisson's ratio are also necessary to simulate a reliable and accurate FEM model.

The default values of 0.1 for the flow potential eccentricity and 0 for the viscosity parameter, which were recommended by the CDP model, were employed. The prediction performance and the accuracy of the model are not remarkably affected by these two parameters (Tao *et al*. 2013b). Even though the ABAQUS user's manual recommends constant values for the CDP model, in the event of some special cases, the default values may not be proper to be used in the model due to the fact that the passively confined concrete has a complex nature (Tao *et al*. 2013b). Because of this reason, the expressions proposed by the other authors for some CDP parameters, which were considered to have remarkable influences on the ultimate strength, were used instead of default values.

$f_{b0}/f_{c0}$ is a parameter that is thought to have a remarkable effect on the model simulation. The default value of 1.16 provided by the ABAQUS user's manual (2014) for $f_{b0}/f_{c0}$ was not used in the model, instead of it, the following expression that was proposed by Papanikolaou and Kappos (2007) derived from the test data collected from 14 studies was used in the determination of $f_{b0}/f_{c0}$ value

$$f_{b0}/f_{c0} = 1.5(f_{c0})^{-0.075} \quad (7)$$

where $f_{b0}$ and $f_{co}$ are the equibiaxial concrete strength and unconfined compressive strength of cylinder concrete ($f_c$'), respectively. The above formula is valid for the cylinder concrete compressive strength range of 30 and 100 MPa.

Another parameter having a remarkable impact on the ultimate axial strength is the $K_c$ parameter by which the yield surface of the concrete plasticity model is determined.

This parameter is interpreted as the ratio of the second stress invariant on the tensile meridian to that on the compressive meridian (Tao *et al*. 2013b), and its value all the time ranges between 0.5 and 1.0 (Seow and Swaddiwudhipong 2005). When the value of the $K_c$ parameter is 1.0, a circular deviatoric cross-section is acquired for the failure surface and the strength hypothesis in the classic Drucker Prager model uses this condition as well (Kmiecik and Kaminski 2011). However, in the CDP model, the $K_c$ parameter with the value of 2/3 is suggested to be used and this condition of the deviatoric cross-section of failure surface is similar to the strength criterion formulated by William and Warnke (1975). Apart from these, Tao *et al*. (2013b) explored the effect of the $K_c$ parameter on the load-strain curves of two specimens taken from the experimental study of Tomii *et al*. (1977) and it was reported that no effect of the $K_c$ parameter on the initial stage of the load-strain curves was observed whereas the significant effect of the $K_c$ parameter was beheld after the column yielded. Additionally, it was stated that diminishing the $K_c$ parameter increased the ultimate strength. These findings emphasize that the determination of the $K_c$ parameter should be done carefully. The following expression, which was deduced by Tao *et al*. (2013b) with respect to Yu *et al*. (2010), was used in the determination of the $K_c$ parameter

$$K_c = \frac{5.5}{5 + 2(f_c')^{0.075}} \tag{8}$$

To represent the plastic flow potential of confined concrete, the dilation angle ($\psi$), which is the measured inclination angle in the meridional plane of the failure surface towards the hydrostatic axis, should be properly decided. Because in the literature, various values for ψ were used by many researchers (Xiong and Zha 2007, Papanikolaou and Kappos 2007). In ABAQUS CAE (2014), the permitted range for $\psi$ value is between 0 and 56°, however, the value of $\psi$ could not be used as 0° in ABAQUS CAE that means it should be computed more than 0°. Tao *et al*. (2013b) also performed a sensitivity analysis on the impact of $\psi$ on the ultimate strength and load versus strain curve of specimens obtained from the experimental study of Tomii *et al*. (1977). It was expressed that the higher $\psi$ value resulted in the higher ultimate strength whereas the initial part of the load-strain curve was not influenced by $\psi$ values. The reason underlies the higher ultimate strength achieved by increasing the value of $\psi$ is that the dilation angle is directly related to the interaction between the concrete and steel tube and increasing the dilation angle increases the concrete dilation rate that led to the establishment of a stronger interaction between the concrete and steel tube. Since the ultimate strength of the model in ABAQUS is affected by $\psi$ value, an accurate value of $\psi$ should be determined at the first. Tao *et al*. (2013b) proposed an equation by using regression analysis as a function of confinement factor that has strict relation with dilation of concrete. This equation presented as follow was used in the determination of dilation angle

$$\Psi = \begin{cases} 56.3(1-\xi_c) & for\ \xi_c \le 0.5 \\ 6.672e^{\frac{7.4}{4.64+\xi_c}} & for\ \xi_c > 0.5 \end{cases} \tag{9}$$

where $\xi_c$ is the confinement factor and to be determined by the following expression

$$\xi_c = \alpha_n \frac{f_{sy}}{f_{ck}} \tag{10}$$

where $\alpha_n$ and $f_{ck}$ are the nominal steel ratio of CFST and CFDST columns and the concrete characteristic compressive strength, respectively, to be determined following equations

$$\alpha_n = \frac{A_s}{A_{c,nominal}} \tag{10a}$$

where $A_{c,nominal}$ is the nominal cross-sectional area of the concrete and to be determined as follows

$$A_{c,nominal} = \frac{\pi(D-2t)^2}{4} \tag{10b}$$

where $D$ and $t$ are the diameter and thickness of the steel tube, respectively.

$$f_{ck} = 0.67 f_{cu} \tag{10c}$$

and where $f_{cu}$ is the concrete characteristic cube strength. It should be stated that in the case of CFDST columns, only the outer steel tube should be considered in the confinement factor calculation.

It was articulated by Tao *et al*. (2013b) that the tensile characteristic of concrete does not play a critical role on the CFST stub columns when they are under the axial compression loading condition. Yet, the tensile behavior of concrete has to be defined in the model generated on ABAQUS CAE software when the CDP model is handled to describe the concrete material. In this study, the following expression was used to describe the uniaxial tensile response of concrete (CEBFIP 1993) that assumes a linear stress-strain behavior until the ultimate tensile strength of concrete was achieved

$$f_{ctm} = \begin{cases} 0.3x(f_c')^{2/3} & for\ concrete\ class \le C50/60 \\ 2.12xln\left(1+\frac{f_{cm}}{10}\right) & for\ concrete\ class > C50/60 \end{cases} \tag{11}$$

where $f_{ctm}$ and $f_{cm}$ are the mean tensile strength and mean compressive strength, respectively. According to Eurocode 2 (EC2) (2004), the mean compressive strength can be calculated by the following expression

$$f_{cm} = f_c' + 8 \tag{11a}$$

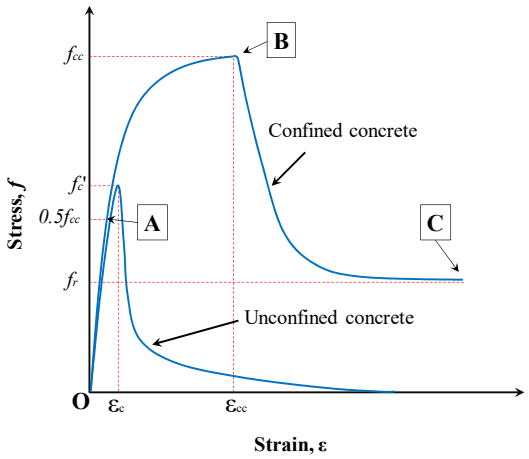


Fig. 4 Stress-strain curves for the confined and unconfined concrete (Hu *et al*. 2003, Binici 2005)

The fracture energy was used to describe the tensile softening characteristic of concrete and the following expression was utilized in the calculation of fracture energy (Bažant and Becq-Giraudon 2002, CEBFIP 2003)

$$G_F = (0.0469d_{max}^2 - 0.5d_{max} + 26)\left(\frac{f_c'}{10}\right)^{0.7} \quad (12)$$

where $G_F$ and $d_{max}$ are the fracture energy for tensile concrete and maximum coarse aggregate size, respectively. When unconfined cylinder concrete compressive strength ($f_c$') and maximum coarse aggregate size ($d_{max}$) values are computed in the unit of MPa and mm, respectively, the fracture energy ($G_F$) would be in the unit of N/m and if the maximum aggregate size was not provided, it could be taken as 22.5 mm.

In the current model, the stress versus strain curve for confined concrete suggested by Hu *et al*. (2003) was used with an alteration in the softening region as presented in Fig. 4. The model suggested by Hu *et al*. (2003) consists of three regions that could be elucidated as elastic, strain hardening, and linear softening regions. But the model proposed in this study assumes a strain-softening region as opposed to Hu *et al*. (2003) since the confinement of concrete ensured by steel tube would increase the peak strain. Therefore, the function that was suggested by Binici (2005) was used to define the descending branch of confined concrete material. As a result, in this study, as clearly seen from Fig. 4, the proposed model consists of three regions that could be stated as elastic region, which begins from the origin (Point O) and ends at the proportional limit stress (Point A), the strain hardening region, which falls between the proportional limit (Point A) and confined concrete stress (Point B), and strain softening region, falls between the confined concrete stress (Point B) and plateau (Point C). This model for the confined concrete has been developed in order to properly describe the behavior of the concrete material placed in a column having a reducing cross-section.

In Fig. 4, $f_c$', $f_{cc}$ and $f_r$ are the unconfined compressive strength of cylinder concrete, confined compressive strength, and residual stress, respectively. The corresponding strains of unconfined and confined concretes are demonstrated by $\varepsilon_c$ and $\varepsilon_{cc}$, respectively. The compressive strength of cylinder concrete can be obtained by the experimental test and the unconfined concrete strain, $\varepsilon_c$, can be considered as 0.003 regarding ACI (2008) suggestion. Yet, the following equations suggested by Mander *et al*. (1988) was used in the calculation of the confined concrete parameters, such as strength and corresponding strain

$$f_{cc} = f_c' + k_1 f_1 \quad (13)$$

$$\varepsilon_{cc} = \varepsilon_c\left(1 + k_2\frac{f_1}{f_c'}\right) \quad (14)$$

where $k_1$ and $k_2$ are the constants recommended by Richart *et al*. (1928) to be taken as 4.1 and 20.4, respectively, $f_1$ is the lateral confining pressure provided by the steel tube (calculated with Eqs. (15)-(16) recommended by Hu *et al*. (2003).

In the case of $21.7 \le D/t \le 47$

$$f_1 = f_{sy}\left[0.043646 - 0.000832\left(\frac{D}{t}\right)\right] \quad (15)$$

In the case of $47 < D/t \le 150$

$$f_1 = f_{sy}\left[0.006421 - 0.0000357\left(\frac{D}{t}\right)\right] \quad (16)$$

As stated above, in the current model, the proportional limit stress was taken as $0.5f_{cc}$ according to Hu *et al*. (2003) and the corresponding strain was calculated by dividing the proportional limit stress to confined concrete's modulus of elasticity, $E_{cc}$. The empirical equation given as follows and suggested by ACI (2008) was used to determine the acceptably elastic modulus for the confined concrete (Eq. (17)). In addition to that, the Poisson's ratio for conventional concrete, $v_c$, ranges between 0.15 and 0.22 and it was presumed to be 0.2 for the confined concrete in this numerical analysis.

$$E_{cc} = 4700\sqrt{f_{cc}} \quad (17)$$

The strain hardening region of the stress versus strain curve of the confined concrete was determined by the following formula that was recommended by Sanez (1964)

$$f_1' = \frac{E_{cc}\varepsilon_1'}{1 + (R + R_E - 2)\left(\frac{\varepsilon_1'}{\varepsilon_{cc}}\right) - (2R - 1)\left(\frac{\varepsilon_1'}{\varepsilon_{cc}}\right)^2 + R\left(\frac{\varepsilon_1'}{\varepsilon_{cc}}\right)^3} \quad (18)$$

where $f_1$' and $\varepsilon_1$' is the stress and strain in the strain hardening region of confined concrete, respectively, $R$ and $R_E$ are the coefficients to be calculated by the following

expressions

$$R = \frac{R_E(R_\sigma - 1)}{(R_\varepsilon - 1)^2} - \frac{1}{R_\varepsilon} \tag{18a}$$

$$R_E = \frac{E_{cc}\varepsilon_{cc}}{f_{cc}} \tag{18b}$$

and where $R_\sigma$ and $R_\varepsilon$ are set to be equivalent to 4 according to the suggestion by Hu and Schnobrich (1989).

In this situation, in the formula proposed by Sanez (1964), only the strain, $\varepsilon$, value is unknown in order to calculate the stress. The stress values for the strain hardening region could be easily computed by postulating the strain values which must be between the proportional strain and the confined strain.

To achieve the last region of the stress-strain curve for confined concrete, the function by Binici (2005) was handled as follows

$$f_2' = f_r + (f_c' - f_r)exp\left[-\left(\frac{\varepsilon_2' - \varepsilon_{cc}}{\alpha}\right)^\beta\right] \quad in\ the\ case\ of\ \varepsilon \geq \varepsilon_{cc} \tag{19}$$

where $f_2$' and $\varepsilon_2$' are the stress and strain in the strain-softening region of confined concrete, respectively, $\alpha$ and $\beta$ are the parameters appointing the descending branch shape. Following equations stated as a function of $\xi_c$ were used to determine the residual stress ($f_r$) and parameter $\alpha$ (Eqs. (20)-(21), respectively) whereas the parameter $\beta$ can be set to be equivalent to 1.2

$$f_r = 0.7\left(1 - e^{-1.38\xi_c}\right)f_c' \leq 0.25f_c' \tag{20}$$

$$\alpha = 0.04 - \frac{0.036}{1 + e^{6.08\xi_c - 3.49}} \tag{21}$$

It is noted that $f_r$, $\alpha$, and $\beta$ cannot be directly attained from the test, they were achieved by various trials giving the best-fit values (Tao *et al*. 2013b).

### 2.2 Interaction and surface identifications

In the modeling of each specimen, endplates, which were placed at the top and bottom of columns, were used so as to attain equal contractions. In this way, each CFST composite tapered column specimen consisted of four components such as steel tube, concrete infill, and the top and bottom endplates as delineated in Fig. 5(a) whereas each CFDST specimen composed of five components such as outer and inner steel tubes, concrete annulus, and the top and bottom endplates as given Fig. 5(b). The interactions between the components were identified by adopting their surfaces.

The surface-to-surface contact and Tie constraint available in ABAQUS CAE (2014) were employed to govern the bond between the specimen components. By using these methods, the surfaces should be first identified according to their characterizations namely it should be decided which surface will penetrate the other. For this condition, in ABAQUS CAE (2014), the surfaces can be defined as master or slave. In the current model, the steel tube surfaces were selected as master surfaces during the interaction with concrete whereas they were designated as slave surfaces when interacted with endplates. The surfaces of endplates were treated as master surfaces while the surfaces of the concrete annulus were chosen as slave surfaces in all interactions with other components. Normal and Tangential behaviors were computed for the surface-to-surface contact properties. The pressure-overclosure model with hard contact feature was used for normal behavior whereas the penalty friction model with a friction coefficient of 0.6 and directionality of isotropic was applied for Tangential behavior. In the literature, there are several values considered by many researchers for the friction coefficients such that the value of 0.25 was used by Schneider and Member (1998), 0.30 by Lam *et al*. (2012), 0.4 by Hassanein *et al*. (2013), and 0.6 by Han *et al*. (2007). Since the value 0.6 was agreed by most test results (Rabbat and Russell 1985), this value of the coefficient of friction was chosen. The surface-to-surface contact was designated to identify the interactions between the steel tube(s) and the concrete infill (or annulus) surfaces and also between the endplates and the concrete infill (or annulus) surfaces. Tie constraint, however, was handled to identify only the interactions between the steel tube(s) and endplates surfaces excluding the interaction between the inner steel tube and top endplate. To identify this interaction, the surface-to-surface contact was selected. Lately, the rigid body constraint was adopted for the endplates to prevent their deformations.

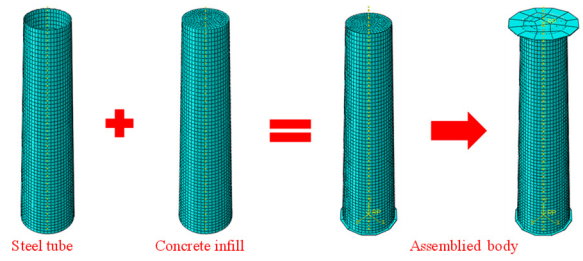


(a) CFST composite tapered column

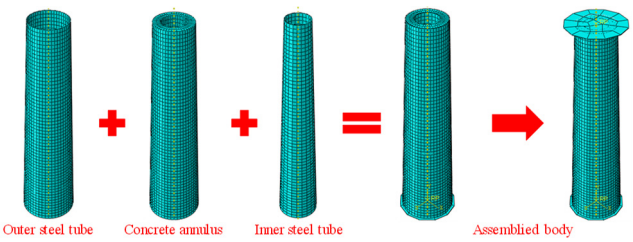


(b) CFDST composite tapered column

Fig. 5 Typical meshing

### 2.3 Finite element type and mesh selection

The components in this study were modeled with respect to the deformable solid shape. The revolution type was used to sketch the solid-shaped components. C3D8 element type with reduced integration and geometric order of linear was utilized for all components of both CFST and CFDST composite tapered columns. The element shape for C3D8 was hexahedron. The approximate global size of the mesh was 24 for steel and concrete components. Yet, the approximate global size of the mesh for endplates was 12 because there is no influence of mesh size of endplates on the results. Moreover, the local seed was applied which was selected as 48 for steel and concrete components and 12 for endplates. Figs. 5(a)-(b) shows the representative meshing of each component of CFST and CFDST composite tapered columns, respectively.

### 2.4 Boundary and loading conditions

There was a reference (RF) point in the top and bottom endplates in order to specify the center of the plates and as aforementioned to create a rigid body constraint. The boundary and loading were implemented on the specimens from these RF points. Encastre type boundary condition in ABAQUS CAE (2014) was used at the bottom endplates so as to obtain fixed support against all degrees of freedom. However, the top plate on which the load was applied was unrestrained in the loading direction. The nodes that remained in the specimen were free to displace or rotate in any direction. The static uniform loading by designating a displacement on the RF point of the top endplate was applied to each specimen.

However, for the sample that was anticipated to fail due to the buckling such as the CFST composite tapered column specimen from the study of Ren *et al*. (2017), the boundary condition at the bottom was fixed against 4 degrees of freedom ($u_x = u_y = u_z = \theta_y = 0$). In other words, the deformations in the x, y, and z axes, as well as the rotation about the y-axis, were restrained. Namely, the bottom plate of the model was allowed to rotate just about the $x$ and $z$ axes. On the other hand, the top plate on which the load was applied was allowed to deform in the $y$-direction and rotate about the $x$ and $z$ axes. Indeed, the deformations were inhibited in the $x$ and $z$ direction and the rotation was forbidden about the $y$-axis at the top plate ($u_x = u_z = \theta_y = 0$). The loading was applied similar to the aforementioned way.

## 3. Verifying the FEM model

To accurately compute the demeanor of the CFST and CFDST composite tapered columns, the verification and calibration of the proposed model is a crucial point. For this reason, the previously conducted experimental test results were adopted in the verification and calibration of the proposed FEM model.

The experimental test results of two specimens denoted as TC2-1 (TC2-2) and TC3-1 (TC3-2), from the study of Han *et al*. (2010) were utilized in the affirmation of the proposed FEM model. The specimens from this study were the CFST composite tapered column samples manufactured by using the steel tube with a yield strength of 410.1 MPa and the concrete with the average cubic strength at the time of the test of 69.6 MPa. The base diameters of the CFST composite tapered columns, namely, the diameter in section B-B as demonstrated in Fig. 2(a), were kept constant as 200 mm in both test specimens whereas the top diameters of the columns, the diameter in section A-A as demonstrated in Fig. 2(a), were 158 and 116 mm for the specimen labeled as TC2-1 (TC2-2) and TC3-1 (TC3-2) specimens, respectively. It means that the tapered angle for TC2-1 (TC2-2) labeled specimen was 2° while it was 4° for the specimen with the label of TC3-1 (TC3-2) since the height of the CFST composite tapered column specimens was 600 mm. The steel tube thickness was 3.75 mm for all specimens. Besides, the steel tube had the elastic modulus and Poisson's ratio of 195 GPa and 0.279, respectively.

Additionally, from the study of Ren *et al*. (2017), the CFST composite tapered column specimen designated as cc4-1 (cc4-2) was used in the illustration of the estimation capability of the proffered FEM model. In the manufacturing of this specimen, the steel tube with a yield strength of 389.3 MPa and the concrete with the average cubic strength at the time of the test of 62.8 MPa were utilized. The base diameter of the CFST composite tapered column, namely, the diameter in section B-B as demonstrated in Fig. 2(a), was 200 mm while the top diameter of the column, the diameter in section A-A as demonstrated in Fig. 2(a), was 170 mm for this specimen. In this way, the tapered angle value was 0.57° because this CFST composite tapered column specimen had a height of 1500 mm. The thickness of the steel tube was 2.92 mm. Besides, the steel tube had the elastic modulus and Poisson's ratio of 206 GPa and 0.294, respectively.

Likewise, four CFDST composite tapered column specimens experimentally tested by Li *et al*. (2012) were used to indicate the prediction performance of the proffered FEM model. The specimens were designated as C2-1 (C2-2), C3-1 (C3-2), C4-1 (C4-2), and C5-1 (C5-2). In this study of Li *et al*. (2012), all CFDST composite tapered columns were manufactured by the outer steel tube with a yield strength of 439.3 MPa, inner steel tube with a yield strength of 396.5 MPa, and the concrete with the average cubic strength at the time of the test of 52.5 MPa. The base outer steel tube diameters of the CFDST composite tapered columns, namely, the outer diameter in section B-B as demonstrated in Fig. 2(b), were 350 mm for both C2-1 (C2-2) and C3-1 (C3-2) specimens whereas it was 300 and 250 mm for the specimen designated as C4-1 (C4-2) and C5-1 (C5-2), respectively. The top outer steel tube diameters of the columns, namely, the outer diameter in section A-A as delineated in Fig. 2(b), were 329, 308, 282, and 235 mm for the specimens labeled as C2-1 (C2-2), C3-1 (C3-2), C4-1 (C4-2), and C5-1 (C5-2), respectively. The base inner steel tube diameters, namely, the inner diameter in section B-B as demonstrated in Fig. 2(b), were 231 mm for both C2-1 (C2-2) and C3-1 (C3-2) specimens whereas it was 198 and 165 mm for the specimens designated as C4-1 (C4-2) and C5-1 (C5-2), respectively. The top inner steel tube diameters of

the columns, namely the outer diameter in section A-A as delineated in Fig. 2(b), were 210, 189, 180, and 150 mm for the specimens labeled as C2-1 (C2-2), C3-1 (C3-2), C4-1 (C4-2), and C5-1 (C5-2), respectively. The tapered angles for these CFDST composite tapered column specimens were 0.57° for the specimens labeled as C2-1 (C2-2), C4-1 (C4-2), and C5-1 (C5-2) while it was 1.14° for the C3-1 (C3-2) denoted specimen. Since the height of the column specimens was 1050 mm for C2-1 (C2-2) and C3-1 (C3-2) named samples, 900 mm for C4-1 (C4-2) named sample, and 750 mm for C5-1 (C5-2) named sample. The thicknesses of the outer and inner steel tubes used in the manufacturing of the CFDST composite tapered columns were 3.82 and 2.92 mm, respectively. Moreover, the outer steel tube had the elastic modulus and Poisson's ratio of 212 GPa and 0.307, respectively, while the inner steel tube had 202 GPa and 0.295, respectively.

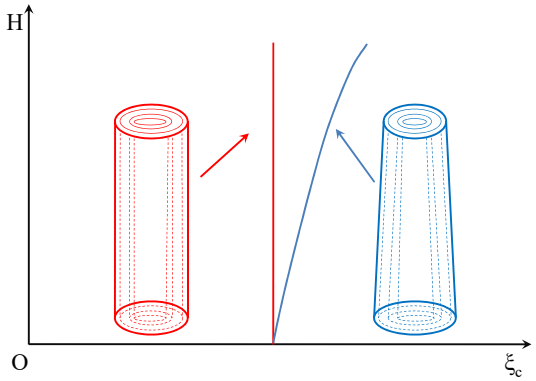


Fig. 6 Schematically illustration of the relation between confinement factor and height of CFDST composite straight and tapered columns (Li et al., 2012)

In addition, two CFDST composite tapered column specimens experimentally tested by Han *et al*. (2011) were used in the verification of the model. TC1-1 (TC1-2) and TC2-1 (TC2-2) labeled specimens from the study of Han *et al*. (2011) had the outer and inner steel tube yield strength values of 319.6 and 380.6 MPa, respectively. The concrete used between the steel tubes had an average cubic strength at the time of the test of 65.6 MPa. The outer and inner steel tube thicknesses were 3.62 and 3.72 mm, respectively. The base outer steel tube diameters of the CFDST composite tapered columns, namely, the outer diameter in section B-B as demonstrated in Fig. 2(b), were 220 mm for both TC1-1 (TC1-2) and TC2-1 (TC2-2) specimens whereas the top outer steel tube diameter of the columns, namely, the outer diameter in section A-A as delineated in Fig. 2(b), was 197 mm. The base inner steel tube diameters, namely, the inner diameter in section B-B as demonstrated in Fig. 2(b), were 159 and 106 mm for TC1-1 (TC1-2) and TC2-1 (TC2-2) specimens, respectively, whereas it was 136 and 83 mm for the top inner steel tube diameters of the TC1-1 (TC1-2) and TC2-1 (TC2-2) labeled column specimens, respectively, namely the outer diameter in section A-A as delineated in Fig. 2(b). The column height was 660 mm and in this way,

Table 1 Experimental dataset handled in the verification of the model

| Reference | Sample label | Outer steel tube [$D$ x $t_o$ (mm x mm)] | | Inner steel tube [$d$ x $t_i$ (mm x mm)] | | Steel tube yield strength [$f_{sy}$ (MPa)] | | Concrete compressive strength [$f_{cu}$ (MPa)] | Height of specimen [$H$ (mm)] |
|---|---|---|---|---|---|---|---|---|---|
| | | Section A-A | Section B-B | Section A-A | Section B-B | Outer | Inner | | |
| Han *et al.* (2010) | TC2-1* | 158 × 3.75 | 200 × 3.75 | - | - | 410.1 | - | 69.6 | 600 |
| | TC2-2* | 158 × 3.75 | 200 × 3.75 | - | - | 410.1 | - | 69.6 | 600 |
| | TC3-1* | 116 × 3.75 | 200 × 3.75 | - | - | 410.1 | - | 69.6 | 600 |
| | TC3-2* | 116 × 3.75 | 200 × 3.75 | - | - | 410.1 | - | 69.6 | 600 |
| Ren *et al.* (2017) | cc4-1* | 170 × 2.92 | 200 × 2.92 | - | - | 389.3 | - | 62.8 | 1500 |
| | cc4-2* | 170 × 2.92 | 200 × 2.92 | - | - | 389.3 | - | 62.8 | 1500 |
| Li *et al.* (2012) | C2-1** | 329 × 3.82 | 350 × 3.82 | 210 × 2.92 | 231 × 2.92 | 439.3 | 396.5 | 52.5 | 1050 |
| | C2-2** | 329 × 3.82 | 350 × 3.82 | 210 × 2.92 | 231 × 2.92 | 439.3 | 396.5 | 52.5 | 1050 |
| | C3-1** | 308 × 3.82 | 350 × 3.82 | 189 × 2.92 | 231 × 2.92 | 439.3 | 396.5 | 52.5 | 1050 |
| | C3-2** | 308 × 3.82 | 350 × 3.82 | 189 × 2.92 | 231 × 2.92 | 439.3 | 396.5 | 52.5 | 1050 |
| | C4-1** | 282 × 3.82 | 300 × 3.82 | 180 × 2.92 | 198 × 2.92 | 439.3 | 396.5 | 52.5 | 900 |
| | C4-2** | 282 × 3.82 | 300 × 3.82 | 180 × 2.92 | 198 × 2.92 | 439.3 | 396.5 | 52.5 | 900 |
| | C5-1** | 235 × 3.82 | 250 × 3.82 | 150 × 2.92 | 165 × 2.92 | 439.3 | 396.5 | 52.5 | 750 |
| | C5-2** | 235 × 3.82 | 250 × 3.82 | 150 × 2.92 | 165 × 2.92 | 439.3 | 396.5 | 52.5 | 750 |
| Han *et al.* (2011) | TC1-1** | 197 × 3.62 | 220 × 3.62 | 136 × 3.72 | 159 × 3.72 | 319.6 | 380.6 | 65.6 | 660 |
| | TC1-2** | 197 × 3.62 | 220 × 3.62 | 136 × 3.72 | 159 × 3.72 | 319.6 | 380.6 | 65.6 | 660 |
| | TC2-1** | 197 × 3.62 | 220 × 3.62 | 83 × 3.72 | 106 × 3.72 | 319.6 | 380.6 | 65.6 | 660 |
| | TC2-2** | 197 × 3.62 | 220 × 3.62 | 83 × 3.72 | 106 × 3.72 | 319.6 | 380.6 | 65.6 | 660 |

*CFST column samples; ** CFDST column samples

the tapered angle was 1° for both CFDST composite tapered column specimens. Furthermore, the outer steel tube had the elastic modulus and Poisson's ratio of 201 GPa and 0.286, respectively, while the inner steel tube had 192 GPa and 0.282, respectively.

The details of the test specimens are also elaborately submitted in Table 1. In the studies mentioned above, two samples were produced from each specimen and the results of both were submitted. However, in this study, the average of both sample results was compared with the outcome of the FEM model. Besides, since the cross-section of the CFST and CFDST composite tapered columns diminishes from bottom to top, in this study, two different simulations were conducted for the CFST and CFDST composite columns with respect to the top and bottom cross-sections. In other words, for each composite tapered column specimen, the calculations of the material definition of concrete were carried out taking into consideration the confinement factor determined according to the bottom and top cross-sections. This assessment was done due to the fact that the confinement factor is directly related to the (outer) steel tube diameter and it is not constant in tapered columns.

Fig. 6 is presented in order to indicate this relation between the confinement effect and the height of CFDST composite straight and tapered columns. It can be overtly seen from Fig. 6 that in the CFDST composite straight column, the confinement effect provided by the outer steel tube remains constant throughout its height whereas, in the CFDST composite tapered columns, the outer steel tube provides more confinement as its diameter reduces. In another saying, decreasing the cross-section of the tapered column enhances the confinement effect provided by the outer steel tube, thus meaning the tapered steel tube provides more confinement to the concrete on the top section (Li *et al*. 2012). Additionally, a similar relationship between the cross-section and the height of the column can be observed in the CFST type tapered columns.

The predicted ultimate axial strength values by using the developed FEM model regarding the CFST and CFDST composite tapered columns are given in Tables 2 and 3, respectively. The tables involve both the predicted ultimate axial strength values taking into consideration the confinement effect determined regarding the top and bottom cross-sections. The abbreviation $N_{u,EXP}$ was used to demonstrate the experimental ultimate axial strength while $N_{u,FEM}$ was utilized to indicate the computed ultimate axial strength by using the proposed FEM model. The symbols '*A* and *B*', which were used with $N_{u,FEM}$, were handled to show the predicted ultimate axial strength values by using the confinement effect determined according to section A-A and B-B as presented in Fig. 2, respectively. Besides, the normalized values of the predicted ultimate axial strength are depicted in Tables 2 and 3. The results indicated that the proposed FEM model has superior prediction performance for both CFST and CFDST composite tapered columns. The predicted ultimate axial strength values were near to that obtained from the experimental test. As can be clearly seen from Table 2, the model was suitable not only for the CFST composite tapered stub columns but also for slender columns, which was experimentally tested by Ren *et al*. (2017). The results also showed that the prediction performance of the proposed model can be acceptable for the confinement effect determined with respect to sections A-A and B-B. To graphically illustrate the prediction capability of the developed FEM model, the predicted versus experimental ultimate axial strength values of CFST and CFDST composite tapered columns are given in Fig. 7. Fig. 7(a) indicates the predicted ultimate axial strength values of CFST and CFDST composite tapered columns regarding the confinement effect determined by taking into consideration section A-A whereas Fig. 7(b) illustrates the predicted ultimate axial strength considering section B-B. It could be overtly seen that the predicted ultimate axial strength values of both conditions amass around the 100% agreement line that is the indication of good estimation capableness of the developed FEM model.

The outward buckling of steel tube in the CFST and outer steel tube in CFDST composite tapered columns were observed by many researchers (Li *et al*. 2012, Han *et al*. 2010, 2011, Ren *et al*. 2017). The tapered columns tested in these studies always performed the ductile behavior and the outward buckling of (outer) steel tube occurred at a place near to top section. As reportedly, the failure mode characteristics of CFDST composite tapered stub columns are similar to that of CFST tapered stub columns (Li *et al*.

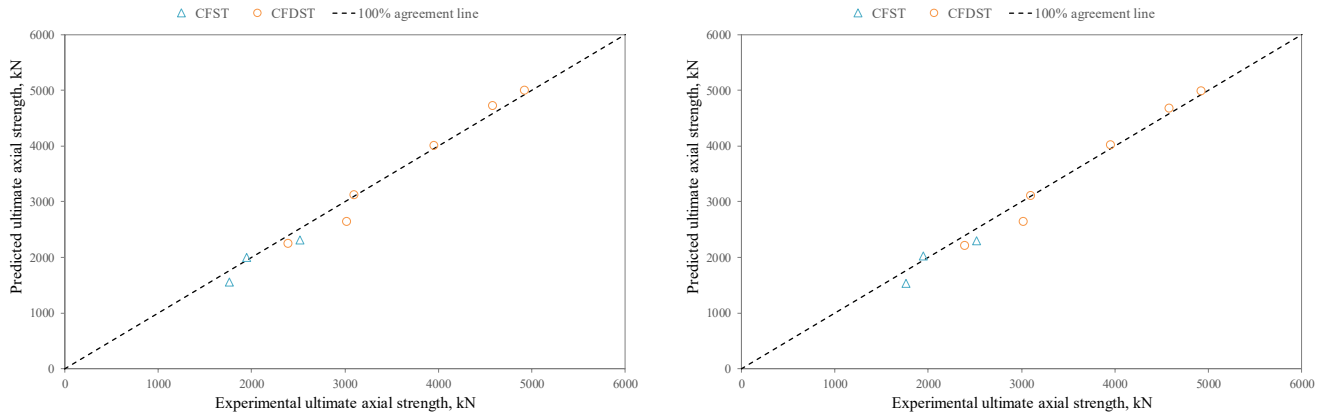


(a) According to section A-A of the tapered column

(b) According to section B-B of the tapered column

Fig. 7 Predicted versus experimental ultimate axial strengths

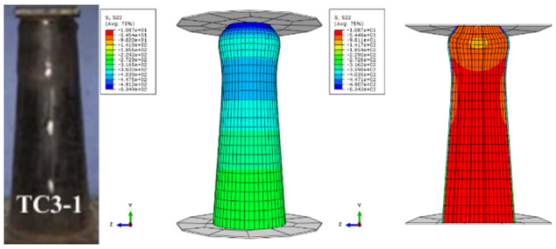


(a) For TC3-1 (Han *et al*. 2010) labeled sample

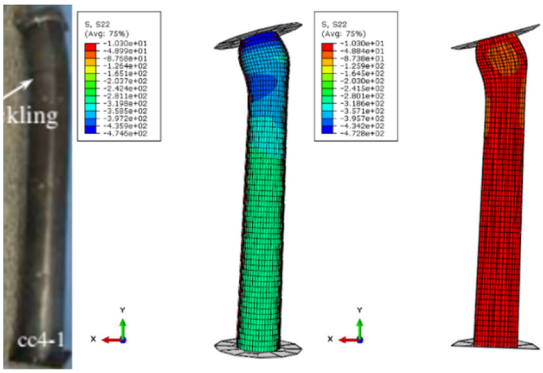


(b) For cc4-1 (Ren *et al*. 2017) labeled sample

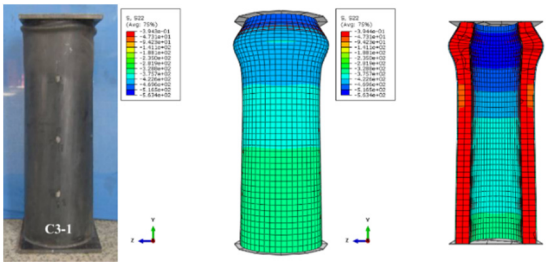


(c) For C3-1 (Li *et al*. 2012) labeled sample

Fig. 8 Typical experimental failure modes and predicted ones by the proposed FEM model3

2012). Typical failure modes were obtained from the experimental test for samples labeled as TC3-1 (Han *et al*. 2010), cc4-1 (Ren *et al*. 2017), and C3-1 (Li *et al*. 2012) are submitted in Figs. 8(a)-(c), respectively. The failure modes achieved from the FEM model for these samples are also given in these figures and when these figures are observed, it would be clearly pointed out that the computed failure modes are almost the same as the actual failure modes. This indicates that the proposed FEM model does not only predict the load-carrying capacity of such composite tapered columns but also simulates their behavior under axial loading and failure mode.

Additionally, the average normalized ultimate axial strength values of 0.944 and 0.976 for the CFST and CFDST composite tapered columns, respectively, as shown at the end of Tables 2 and 3 were achieved when the confinement effect was determined regarding sections A-A. These values were 0.942 and 0.972 when the analysis was carried out with respect to section B-B. Furthermore, the tables include the coefficient of variations (CoV) values of the normalized ultimate axial strength values for both types of composite tapered columns. When the average and COV values of normalized ultimate axial strength of columns are considered, it can be easily comprehended that the developed FEM model has a good prediction performance no matter which section is regarded in the confinement effect determination.

Moreover, the estimation capability of the proposed FEM model was statistically evaluated in terms of mean absolute percent error (MAPE), mean square error (MSE), and root mean square error (RMSE) values. The MAPE, MSE, and RMSE were calculated by using Eqs. (22)-(24), respectively. Tables 2 and 3 also include the MAPE, MSE, and RMSE values of the ultimate axial strengths of CFST and CFDST composite tapered columns, respectively. All these statistical parameters give the amount of error that occurs during the prediction. For this reason, the model with lower error occurrence especially in the case of considering the MAPE is generally purposed in these types of studies since the error value near zero means the perfect estimation capability of the model. The lower MSE and RMSE values are also desired situations in the predictive models, yet, if the value that is aimed to be predicted is high, this would lead to higher MSE and RMSE values. Therefore, only the MAPE with the low value may lonely

Table 2 Prediction performance of the proposed FEM model for CFST column samples

| Reference | Sample label | $N_{u,EXP}$ (kN) | Ave. | $N_{u,FEM-A}$ (kN) | $N_{u,FEM-B}$ (kN) | $N_{u,FEM-A}$/ $N_{u,EXP}$ | $N_{u,FEM-B}$/ $N_{u,EXP}$ |
|---|---|---|---|---|---|---|---|
| Han *et al*. (2010) | TC2-1 | 2574 | 2515 | 2316 | 2299 | 0.921 | 0.914 |
| | TC2-2 | 2456 | | | | | |
| | TC3-1 | 1785 | 1759 | 1552 | 1534 | 0.882 | 0.872 |
| | TC3-2 | 1733 | | | | | |
| Ren *et al*. (2017) | cc4-1 | 1932 | 1948 | 2005 | 2027 | 1.029 | 1.041 |
| | cc4-2 | 1963 | | | | | |
| ***Average*** | | | | | | **0.944** | **0.942** |
| ***COV*** | | | | | | **0.081** | **0.093** |
| ***MAPE*** | | | | **7.53** | **8.48** | | |
| ***MSE*** | | | | **28567** | **34507** | | |
| ***RMSE*** | | | | **169.0** | **185.8** | | |

Table 3 Prediction performance of the proposed FEM model for CFDST column samples

| Reference | Sample label | $N_{u,EXP}$ (kN) | Ave. | $N_{u,FEM-A}$ (kN) | $N_{u,FEM-B}$ (kN) | $N_{u,FEM-A}$/ $N_{u,EXP}$ | $N_{u,FEM-B}$/ $N_{u,EXP}$ |
|---|---|---|---|---|---|---|---|
| Li *et al*. (2012) | C2-1 | 4942 | 4932 | 4997 | 4977 | 1.013 | 1.009 |
| | C2-2 | 4921 | | | | | |
| | C3-1 | 4569 | 4585 | 4714 | 4672 | 1.028 | 1.019 |
| | C3-2 | 4600 | | | | | |
| | C4-1 | 3874 | 3961 | 3998 | 4016 | 1.009 | 1.014 |
| | C4-2 | 4048 | | | | | |
| | C5-1 | 3090 | 3103 | 3113 | 3102 | 1.003 | 1.000 |
| | C5-2 | 3116 | | | | | |
| Han *et al*. (2011) | TC1-1 | 2384 | 2400 | 2235 | 2202 | 0.931 | 0.918 |
| | TC1-2 | 2415 | | | | | |
| | TC2-1 | 3067 | 3022 | 2636 | 2631 | 0.872 | 0.871 |
| | TC2-2 | 2976 | | | | | |
| ***Average*** | | | | | | **0.976** | **0.972** |
| ***COV*** | | | | | | **0.063** | **0.064** |
| ***MAPE*** | | | | **4.17** | **4.24** | | |
| ***MSE*** | | | | **33092** | **34118** | | |
| ***RMSE*** | | | | **181.9** | **184.7** | | |

elucidate the robustness and consistency as well as the power of the proposed model. When the statistical results of the study herein are considered, it can be clearly comprehended that the proposed FEM model has a robust and acceptable as well as strong prediction capability, and its estimation of the ultimate axial strength is reliable and accurate since the MAPE value of both CFST and CFDST composite tapered columns are low and near to each other.

$$MAPE = \frac{1}{n}\sum_{i=1}^{n}\left|\frac{m_i - p_i}{m_i}\right| x100 \quad (22)$$

$$MSE = \frac{\sum_{i=1}^{n}(m_i - p_i)^2}{n} \quad (23)$$

$$RMSE = \sqrt{\frac{\sum_{i=1}^{n}(m_i - p_i)^2}{n}} \quad (24)$$

where $m$ and $p$ are measured ($m_i$) and predicted ($p_i$) values, respectively.

Apart from ultimate axial strength and deformed shape, the FEM also provides the axial load-displacement (or strain) curves. For the CFST tapered column specimens, the

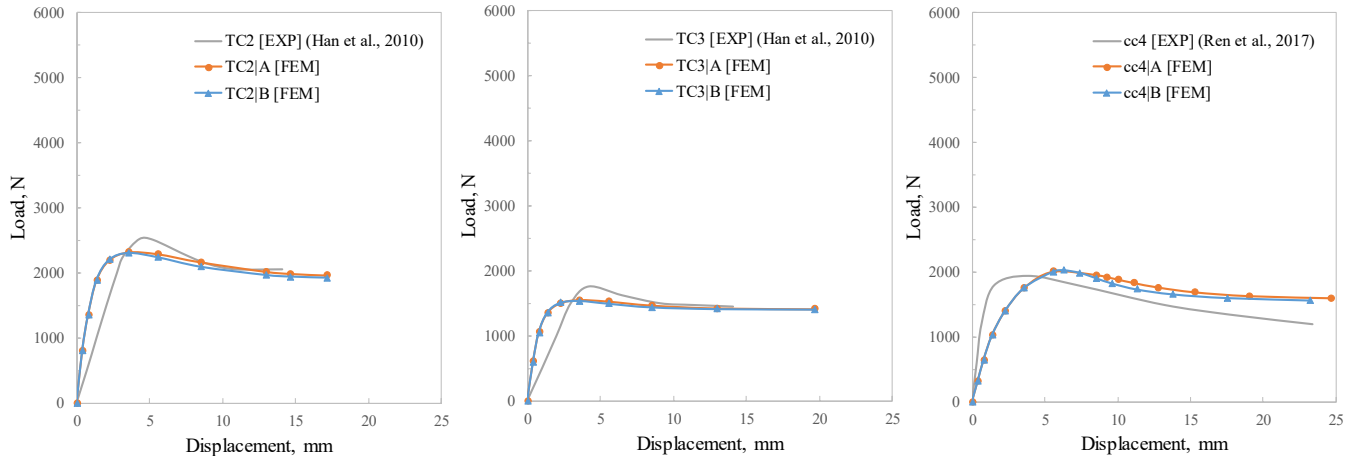


Fig. 9 Comparison of the experimental and computational axial load-displacement of: (a) TC2 and (b) TC3 named CFST tapered specimens from the study of Han *et al*. (2010), and (c) cc4 labeled CFST tapered specimen from the study of Ren *et al*. (2017)

experimental and computational axial load versus displacement curves are displayed in Figs. 9(a)-(c). It has been observed that there are slight differences between the experimental and computational load-displacement curves. Especially, the difference can be seen in the initial stiffness of the columns. For the CFST tapered columns from the study of Han *et al*. (2010), the FEM model resulted in steeper initial stiffness behavior, whereas a more sloping initial stiffness behavior can be observed for the CFST tapered columns taken from the study of Ren *et al*. (2017). On the other hand, a relatively identical behavior has been seen in the descending region for all CFST tapered column specimens.

The experimental and computational axial load versus axial strain curves of the CFDST tapered column specimens obtained from the study of Li *et al*. (2012) are presented in Figs. 10(a)-(d) while the experimental and computational axial load versus axial displacement curves of the CFDST tapered columns taken from the study of Han *et al*. (2011) are shown in Figs. 10(e)-(f). When the load-strain curves for the tapered columns taken from the study of Li *et al*. (2012) are investigated it can be seen that there is a perfect matching in the initial stiffness region of the curves of the CFDST tapered columns. However, in the descending part, generally, the FEM model performed higher values than the experimental. For the axial load versus axial displacement curves of the CFDST tapered column specimens attained from the study of Han *et al*. (2011), the model has yielded a steeper initial stiffness behavior. While the experimental ultimate axial strengths were achieved at higher displacement values, the computational ultimate axial strength values were observed at lower displacement values. This is

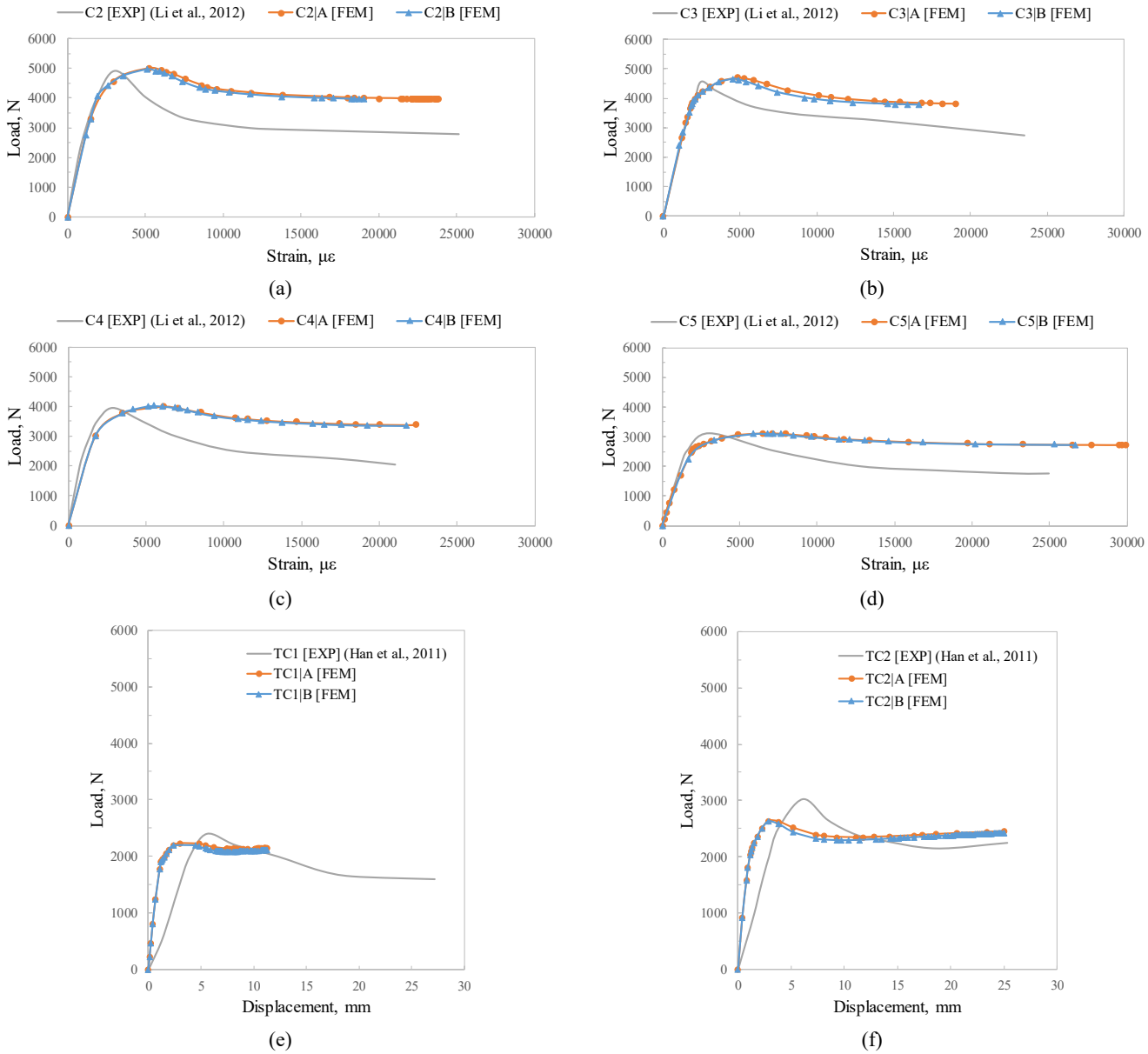


Fig. 10 Comparison of the experimental and computational axial load-displacement of: (a) C2, (b) C3, (c) C4, and (d) C5 named CFDST tapered specimens from the study of Li *et al*. (2012), and (e) TC1 and (f) TC2 labeled CFDST tapered specimens from the study of Han *et al*. (2011)

another difference between the load-displacement curve for the CFDST tapered columns of Han *et al*. (2011). Such discrepancies in these curves have been explained by İpek *et al*. (2021) as the inaccuracies ensued from the lack of modeling the real circumstances containing material strengths, boundary conditions, the precision of the testing devices, initial imperfections, and fabrication errors. In addition, it was emphasized by Hassanein *et al*. (2018) that a fully modeling of all real testing circumstances in the finite element analysis is not possible. Moreover, it was also stated by Yang *et al*. (2008) and Jamaluddin *et al*. (2013) that the concrete characteristics can not only be described by the strength tests even it is taken care of that the concrete strength is measured on the day of testing the column. As a consequence, it can be stated that such types of differences between the real test circumstances and finite element analysis cannot be suppressed. Besides, it can be expressed that despite these discrepancies, the prediction performance of the proposed FEM model for the load-displacement (or strain) behavior can be considered good.

As can be seen in Fig. 9 and Fig. 10, there are two load-displacement (or strain) curves achieved from the FEM model; one was obtained in the case of the concrete confinement determined regarding the section A-A given in Fig. 2, the other one was attained regarding the section B-B presented in the same figure. The initial stiffness behavior of both curves is the same, whereas, after peak strength, the concrete confinement effect determined regarding section B-B has resulted in a lower transitional descending part, but almost the same residual strength part. However, in general, this difference can be neglected, and it can be concluded that the non-uniform cross-section of such tapered columns

Table 4 Properties of CFST columns used in the parametric study

| Sample no | Steel tube [$D \times t$ (mm × mm)] | | Tapered angle [θ (°)] | Steel tube yield strength [$f_{sy}$ (MPa)] | Concrete compressive strength [$f_{cu}$ (MPa)] | Predicted ultimate axial load [$N_{u,FEM}$ (kN)] |
|---|---|---|---|---|---|---|
| | Section | | | | | |
| | A-A | B-B | | | | |
| 1 | 260 × 3 | 360 × 3 | 2.0 | 420 | 40 | 3443 |
| 2 | 280 × 3 | 360 × 3 | 1.6 | 420 | 40 | 3753 |
| 3 | 300 × 3 | 360 × 3 | 1.2 | 420 | 40 | 4202 |
| 4 | 320 × 3 | 360 × 3 | 0.8 | 420 | 40 | 4603 |
| 5 | 340 × 3 | 360 × 3 | 0.4 | 420 | 40 | 4950 |
| 6 | 260 × 3 | 360 × 3 | 2.0 | 420 | 50 | 3762 |
| 7 | 280 × 3 | 360 × 3 | 1.6 | 420 | 50 | 4280 |
| 8 | 300 × 3 | 360 × 3 | 1.2 | 420 | 50 | 4662 |
| 9 | 320 × 3 | 360 × 3 | 0.8 | 420 | 50 | 5184 |
| 10 | 340 × 3 | 360 × 3 | 0.4 | 420 | 50 | 5442 |
| 11 | 260 × 3 | 360 × 3 | 2.0 | 420 | 60 | 4105 |
| 12 | 280 × 3 | 360 × 3 | 1.6 | 420 | 60 | 4619 |
| 13 | 300 × 3 | 360 × 3 | 1.2 | 420 | 60 | 5121 |
| 14 | 320 × 3 | 360 × 3 | 0.8 | 420 | 60 | 5809 |
| 15 | 340 × 3 | 360 × 3 | 0.4 | 420 | 60 | 6084 |
| 16 | 260 × 3 | 360 × 3 | 2.0 | 520 | 40 | 3849 |
| 17 | 280 × 3 | 360 × 3 | 1.6 | 520 | 40 | 4250 |
| 18 | 300 × 3 | 360 × 3 | 1.2 | 520 | 40 | 4672 |
| 19 | 320 × 3 | 360 × 3 | 0.8 | 520 | 40 | 5028 |
| 20 | 340 × 3 | 360 × 3 | 0.4 | 520 | 40 | 5485 |
| 21 | 260 × 3 | 360 × 3 | 2.0 | 520 | 50 | 4238 |
| 22 | 280 × 3 | 360 × 3 | 1.6 | 520 | 50 | 4689 |
| 23 | 300 × 3 | 360 × 3 | 1.2 | 520 | 50 | 5199 |
| 24 | 320 × 3 | 360 × 3 | 0.8 | 520 | 50 | 5582 |
| 25 | 340 × 3 | 360 × 3 | 0.4 | 520 | 50 | 6122 |
| 26 | 260 × 3 | 360 × 3 | 2.0 | 520 | 60 | 4517 |
| 27 | 280 × 3 | 360 × 3 | 1.6 | 520 | 60 | 5165 |
| 28 | 300 × 3 | 360 × 3 | 1.2 | 520 | 60 | 5521 |
| 29 | 320 × 3 | 360 × 3 | 0.8 | 520 | 60 | 6074 |
| 30 | 340 × 3 | 360 × 3 | 0.4 | 520 | 60 | 6648 |

Table 5 Properties of CFDST columns used in the parametric study

| Sample no | Outer steel tube [$Dxt_o$ (mm $x$ mm)] | | Inner steel tube [$dxt_i$ (mm $x$ mm)] | | Tapered angle [θ (°)] | Steel tube yield strength [$f_{sy}$ (MPa)] | | Concrete compressive strength [$f_{cu}$ (MPa)] | Predicted ultimate axial load [$N_{u,FEM}$ (kN)] |
|---|---|---|---|---|---|---|---|---|---|
| | Section | | Section | | | Outer | Inner | | |
| | A-A | B-B | A-A | B-B | | | | | |
| 1 | 260 × 3 | 360 × 3 | 160 × 3 | 260 × 3 | 2.0 | 420 | 420 | 40 | 2970 |
| 2 | 280 × 3 | 360 × 3 | 180 × 3 | 260 × 3 | 1.6 | 420 | 420 | 40 | 3203 |
| 3 | 300 × 3 | 360 × 3 | 200 × 3 | 260 × 3 | 1.2 | 420 | 420 | 40 | 3504 |
| 4 | 320 × 3 | 360 × 3 | 220 × 3 | 260 × 3 | 0.8 | 420 | 420 | 40 | 3753 |
| 5 | 340 × 3 | 360 × 3 | 240 × 3 | 260 × 3 | 0.4 | 420 | 420 | 40 | 3983 |
| 6 | 260 × 3 | 360 × 3 | 160 × 3 | 260 × 3 | 2.0 | 420 | 420 | 50 | 3238 |
| 7 | 280 × 3 | 360 × 3 | 180 × 3 | 260 × 3 | 1.6 | 420 | 420 | 50 | 3511 |
| 8 | 300 × 3 | 360 × 3 | 200 × 3 | 260 × 3 | 1.2 | 420 | 420 | 50 | 3784 |
| 9 | 320 × 3 | 360 × 3 | 220 × 3 | 260 × 3 | 0.8 | 420 | 420 | 50 | 4055 |
| 10 | 340 × 3 | 360 × 3 | 240 × 3 | 260 × 3 | 0.4 | 420 | 420 | 50 | 4307 |
| 11 | 260 × 3 | 360 × 3 | 160 × 3 | 260 × 3 | 2.0 | 420 | 420 | 60 | 3467 |
| 12 | 280 × 3 | 360 × 3 | 180 × 3 | 260 × 3 | 1.6 | 420 | 420 | 60 | 3769 |
| 13 | 300 × 3 | 360 × 3 | 200 × 3 | 260 × 3 | 1.2 | 420 | 420 | 60 | 4061 |
| 14 | 320 × 3 | 360 × 3 | 220 × 3 | 260 × 3 | 0.8 | 420 | 420 | 60 | 4349 |
| 15 | 340 × 3 | 360 × 3 | 240 × 3 | 260 × 3 | 0.4 | 420 | 420 | 60 | 4627 |
| 16 | 260 × 3 | 360 × 3 | 160 × 3 | 260 × 3 | 2.0 | 520 | 520 | 40 | 3461 |
| 17 | 280 × 3 | 360 × 3 | 180 × 3 | 260 × 3 | 1.6 | 520 | 520 | 40 | 3744 |
| 18 | 300 × 3 | 360 × 3 | 200 × 3 | 260 × 3 | 1.2 | 520 | 520 | 40 | 4036 |
| 19 | 320 × 3 | 360 × 3 | 220 × 3 | 260 × 3 | 0.8 | 520 | 520 | 40 | 4321 |
| 20 | 340 × 3 | 360 × 3 | 240 × 3 | 260 × 3 | 0.4 | 520 | 520 | 40 | 4586 |
| 21 | 260 × 3 | 360 × 3 | 160 × 3 | 260 × 3 | 2.0 | 520 | 520 | 50 | 3659 |
| 22 | 280 × 3 | 360 × 3 | 180 × 3 | 260 × 3 | 1.6 | 520 | 520 | 50 | 4008 |
| 23 | 300 × 3 | 360 × 3 | 200 × 3 | 260 × 3 | 1.2 | 520 | 520 | 50 | 4309 |
| 24 | 320 × 3 | 360 × 3 | 220 × 3 | 260 × 3 | 0.8 | 520 | 520 | 50 | 4616 |
| 25 | 340 × 3 | 360 × 3 | 240 × 3 | 260 × 3 | 0.4 | 520 | 520 | 50 | 4905 |
| 26 | 260 × 3 | 360 × 3 | 160 × 3 | 260 × 3 | 2.0 | 520 | 520 | 60 | 3912 |
| 27 | 280 × 3 | 360 × 3 | 180 × 3 | 260 × 3 | 1.6 | 520 | 520 | 60 | 4266 |
| 28 | 300 × 3 | 360 × 3 | 200 × 3 | 260 × 3 | 1.2 | 520 | 520 | 60 | 4596 |
| 29 | 320 × 3 | 360 × 3 | 220 × 3 | 260 × 3 | 0.8 | 520 | 520 | 60 | 4921 |
| 30 | 340 × 3 | 360 × 3 | 240 × 3 | 260 × 3 | 0.4 | 520 | 520 | 60 | 5227 |

has no remarkable influence on the prediction performance of the load-displacement (or strain) curve of the proposed FEM model.

## 4. Parametric study

Based on the verified FEM model, in this section, a total of 60 composite tapered column specimens (covering 30 CFST and 30 CFDST columns) were modeled in order to examine the effect of various parameters (i.e., steel tube yield strength, concrete compressive strength, and tapered angle) on the axial behavior of such columns.

To this aim, two steel tube yield strength values of 420 and 520 MPa, three cubic concrete compressive strength values of 40, 50, and 60 MPa, and five tapered angle values of 0.4, 0.8, 1.2, 1.6, and 2.0 were chosen as variable parameters in this study. As a result, 30 CFST and 30 CFDST composite tapered columns were achieved according to these parameters and the only difference between each CFST and CFDST column sample is that one does not have an inner steel tube whereas the other has. The details of each CFST and CFDST composite tapered column sample are presented in Tables 4 and 5, respectively.

The material definition, surface and interaction identifications, finite element type, mesh selection, and boundary and loading conditions of CFST and CFDST samples were done accordingly as explained in Section 2. The ultimate axial strength of each sample was estimated after modeling by ABAQUS CAE (2014). Since the ultimate axial strength predictions by the models in which

the concrete material was defined according to confinement effect determined regarding sections A-A and B-B were so close to each other in the verification of the proposed FEM model, in the parametric study, the confinement effect provided by steel tube was determined with respect to section B-B. Besides, the confinement effect provided by the steel tube in such columns increases when the height of composite tapered columns increases. For this reason, the model developed according to the lower confinement effect would be more realistic and this condition would be the worst case.

The predicted ultimate axial strength values of CFST and CFDST composite tapered samples are also included in Tables 4 and 5, respectively. Moreover, to visualize the influences of various parameters on the ultimate axial strength, Fig. 11 is plotted. The analysis of the results shows that the CFST composite tapered columns have higher ultimate axial strength values than the CFDST columns. Utilization of inner steel tube, in other words, decreases the concrete amount results in a reduction of ultimate axial strength with the rate ranging between 10 to 35%. Besides, the results indicated that the tapered angle increasing induces the diminishing of ultimate axial strength of both CFST and CFDST composite tapered columns. Increasing the tapered angle from 0.4 to 2.0° reduces the ultimate axial strength of CFST and CFDST composite tapered columns with the rate of about 30 and 25%, respectively.

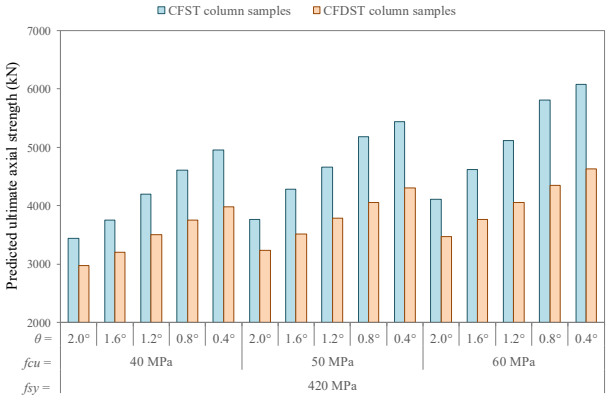


(a) For the steel tube yield strength of 420 MPa

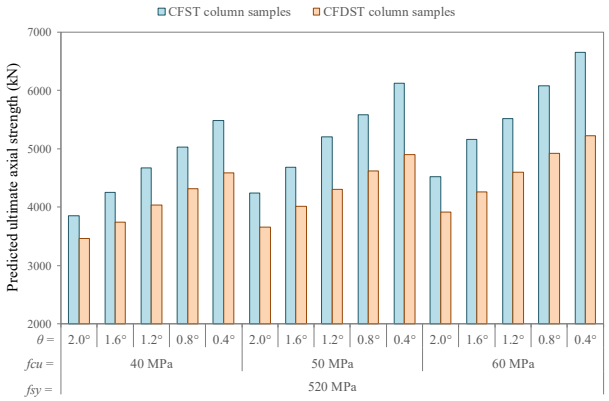


(b) For the steel tube yield strength of 520 MPa

Fig. 11 Variation in the predicted ultimate axial strength of CFST and CFDST composite tapered columns

The strength of materials used in the column production also has a direct impact on the load-carrying capacity of such columns. Using higher concrete strength improves the load-carrying capacity of both CFST and CFDST composite tapered columns. When the compressive strength of cubic concrete is increased from 40 to 60 MPa, the ultimate axial strength of CFST and CFDST tapered columns is also increased with rates of almost 17-23% and 13-18%, respectively. In this context, increasing the yield strength of steel tube(s) also increased the ultimate axial strength of the column. The increment rate owing to the steel tube yield strength increasing was higher in the CFDST tapered columns than the CFST tapered columns. As mentioned above, the variation in the ultimate axial strength of CFST and CFDST composite tapered columns according to the variable parameters is demonstrated in Fig. 11. In Fig. 11(a), the ultimate axial strength is given for the columns manufactured with the steel tube having a yield strength of 420 MPa whilst in Fig. 9(b), the ultimate axial strength is presented regarding the steel tube yield strength of 520 MPa. Figs. 11(a)-(b) obviously demonstrates that increasing the yield strength of steel tube(s) increased the ultimate axial strength of CFST and CFDST composite tapered columns. Yet, it should be noticed that increase in the ultimate axial strength of such composite columns thanks to using materials with higher strength is an expected situation. The main concern in this parametric study is the effect of column type and tapered angle. In the literature, there is no study investigating the ultimate axial strength variation due to the column type but there are limited studies in which the effect of tapered angle was experimentally investigated (Han *et al.* 2010, Li *et al.* 2012). The findings of the tapered angle effect observed in this parametric study were also supported by these experimental researches. For example, Li *et al.* (2012) reported that increasing the tapered angle decreased the ultimate axial strength of the CFDST tapered column. As well, Han *et al.* (2010) mentioned the same influence of tapered angle on CFST tapered column samples. The parametric study results also showed that under the same mechanical and sectional conditions, the CFST tapered columns have higher ultimate axial strength values than the CFDST tapered columns. When a material strength-based discussion is done, it can be stated that the difference between the ultimate axial strength of the CFST and CFDST tapered columns is higher in the case of higher concrete compressive strength, whereas the difference is lower in the case of higher steel tube yield strength.

Apart from the ultimate axial strength, the FEM method gives the relation between the axial load versus the axial displacement of the members. In Figs. 12(a)-(f), the change in the load-displacement behavior of the CFST columns with respect to the tapered angle is presented, whereas, Figs. 13(a)-(f) display the load-displacement behavior of the CFDST column with respect to the tapered angle. When the load-displacement characteristics of the CFST tapered columns are considered, it can be stated that increasing the tapered angle leads to enhance the confinement effect provided by the steel tube, thus resulting in a higher peak strength value. On the other hand, a steeper descending in the post-peak response of the columns can be seen by

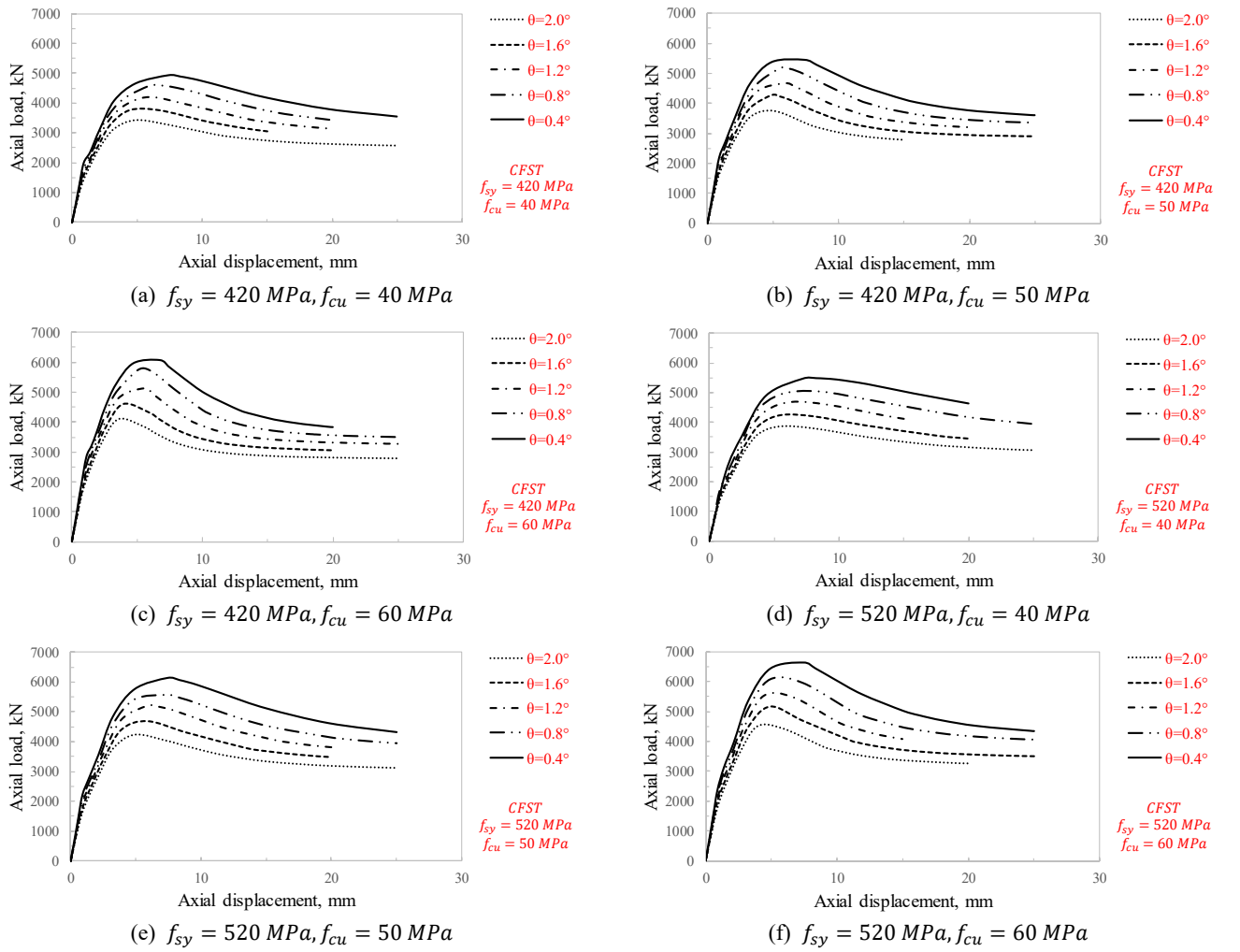


(a) $f_{sy} = 420\ MPa, f_{cu} = 40\ MPa$ (b) $f_{sy} = 420\ MPa, f_{cu} = 50\ MPa$

(c) $f_{sy} = 420\ MPa, f_{cu} = 60\ MPa$ (d) $f_{sy} = 520\ MPa, f_{cu} = 40\ MPa$

(e) $f_{sy} = 520\ MPa, f_{cu} = 50\ MPa$ (f) $f_{sy} = 520\ MPa, f_{cu} = 60\ MPa$

Fig. 12 Axial load versus displacement curves of the CFST tapered columns

increasing the tapered angle. In addition, a slight increase in the initial rigidity of the CFST tapered column was observed when the tapered angle increased. Besides, it can be sighted that the CFST tapered columns having higher tapered angles reach the peak strength at lower displacement levels. Increasing the concrete compressive strength significantly influenced the post-peak behavior of the CFST columns. A remarkably steeper decrease in the load-carrying capacity was observed in the CFST columns having higher compressive strength. In other respects, although increasing the steel tube yield strength increases the load-carrying capacity of the CFST tapered column, no remarkable impact of the steel tube yield strength on the post-peak behavior is observed in the current study. Furthermore, it imperceptibly exerts an influence on the initial stiffness because the elastic modulus of the steel is not impressed by the steel strength.

The load-displacement behaviors of the CFDST tapered columns showed that generally, lower displacement levels are observed in these types of columns. Besides, no significant influence of the tapered angle on the initial rigidity of the columns was observed. As seen in the CFST tapered columns, the CFDST tapered columns having higher tapered angles also reached the peak strength at lower displacement levels, and also, a steeper descending in the post-peak region at a higher tapered angle value was seen. Additionally, the influence of the concrete strength and steel tube yield strength on the load-displacement characteristics of the CFDST tapered columns was identical to in the CFST type columns.

In the final, a local buckling type of failure mode was observed in both CFST and CFDST tapered columns, as exhibited in Figs. 14(a)-(b), respectively. The local buckling was generally detected near the top surface of the column. However, by decreasing the tapered angle, slipping in the location of the buckling through the downward direction was seen. In the CFST tapered columns, the stress in the concrete core is generally developed near the top surface, and thus, the lateral expansion in the concrete caused outward buckling of the steel tube. Thereby, decreasing the tapered angle increased the stress development region in the concrete, thus caused a wider buckling of the steel tube, as can be seen in Fig. 14(a). On the other hand, a different failure mechanism can be seen in the CFDST tapered columns. Since instead of the concrete core, there is an inner steel tube in such types of columns, an outward buckling caused by the shear failure of the concrete annulus occurs. Hence, buckling in the inner steel tube can also be seen. However, decreasing the tapered angle, provide rigidity to the inner steel tube, and thus, the failure

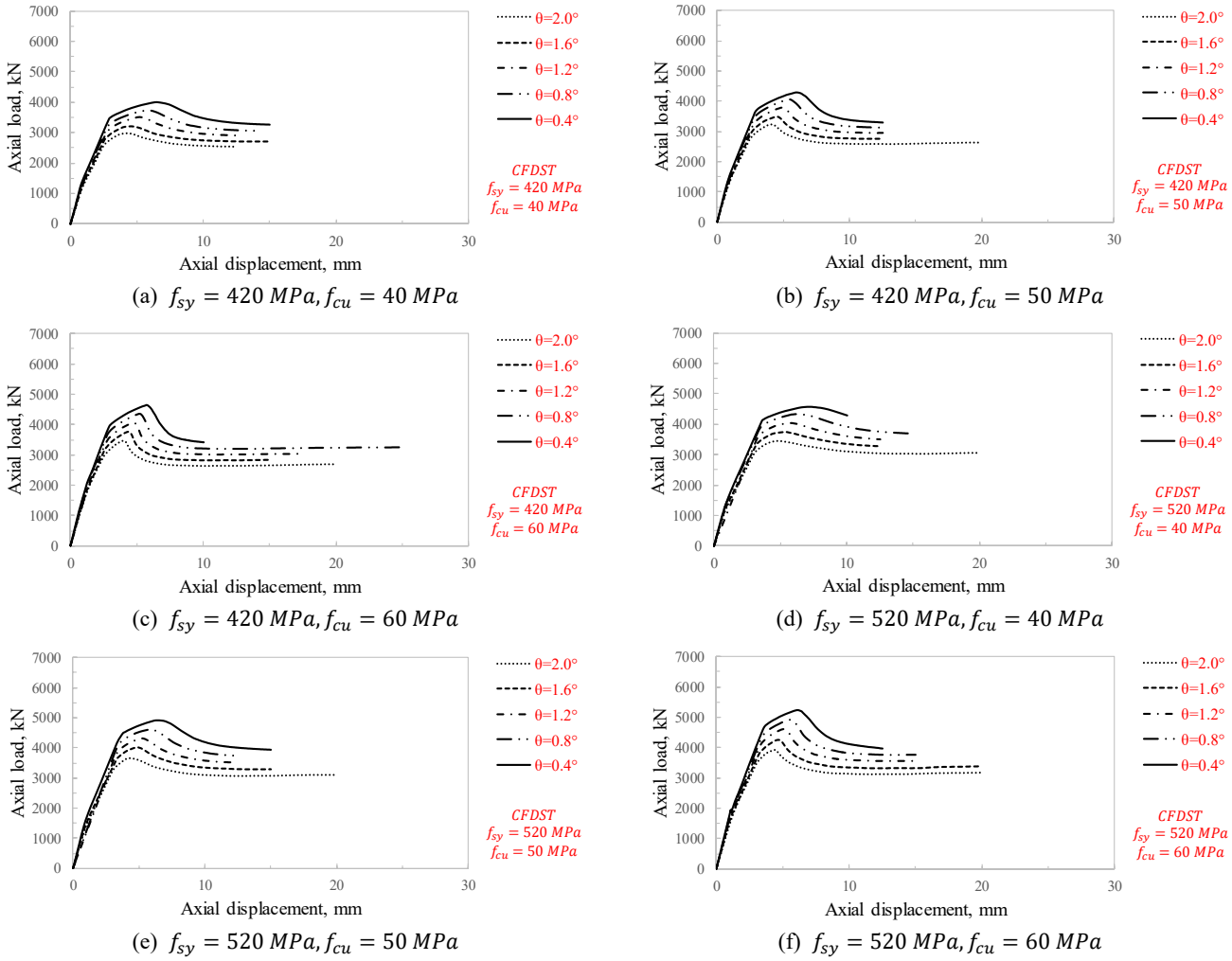


(a) $f_{sy} = 420\ MPa, f_{cu} = 40\ MPa$ (b) $f_{sy} = 420\ MPa, f_{cu} = 50\ MPa$

(c) $f_{sy} = 420\ MPa, f_{cu} = 60\ MPa$ (d) $f_{sy} = 520\ MPa, f_{cu} = 40\ MPa$

(e) $f_{sy} = 520\ MPa, f_{cu} = 50\ MPa$ (f) $f_{sy} = 520\ MPa, f_{cu} = 60\ MPa$

Fig. 13 Axial load versus displacement curves of the CFDST tapered columns

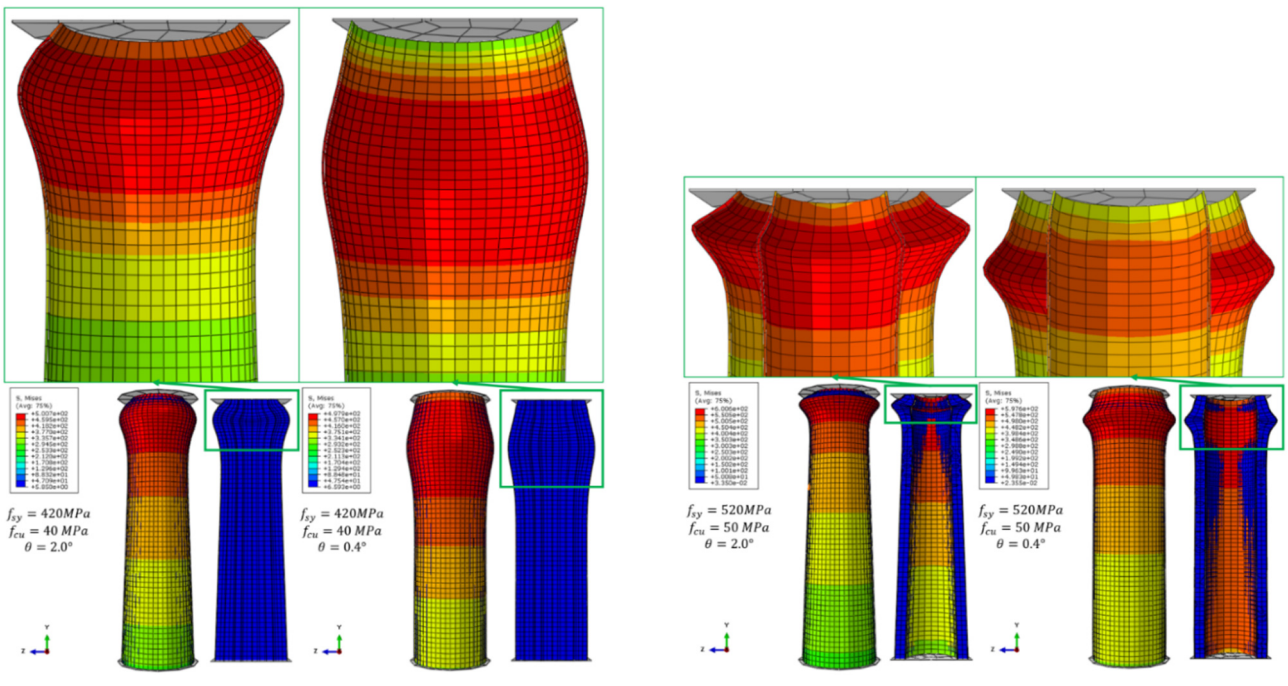


(a) (b)

Fig. 14 Typical failure mode in: (a) CFST tapered columns; and (b) CFDST tapered columns

mechanism in the concrete annulus transform from the shear failure to the lateral expansion, as can be seen in Fig. 14(b).

## 5. Statistical evaluations

The impacts of different parameters on the axial response of the tapered columns were graphically presented in the previous section. Here, the results were statistically evaluated. For this, the analysis of variance (ANOVA) was used to indicate the effectiveness of independent variables on the dependent variable. The analysis method known as general linear model analysis of variance (GLM-ANOVA) was handled in the statistical evaluation of the parametric study results. The software named "Minitab" including the GLM-ANOVA method was employed in performing the statistical analysis. The GLM-ANOVA is a diagnostic tool that decreases the control variance in order to help a control factor dominance to be quantified.

In this study, the tapered angle ($\theta$), steel tube(s) yield strength ($f_{sy}$), and concrete compressive strength ($f_{cu}$) were designated as independent variables while the ultimate axial strength ($N_u$) of the concrete-filled single and double skin steel tubular composite tapered columns was articulated as a dependent variable. Besides, the significance level of 0.05 was adjusted in the analysis to reveal which independent variable is a statistically important parameter on the dependent variable. The results obtained from the statistical analysis of the proposed FEM model are given in Table 6. The significance of the independent parameters can be comprehended taking into consideration the P-values. If the P-value of any independent variable is greater than the level of significance, it can be stated that this variable has an insignificant effect on the dependent variable. On the contrary case, namely, when the P-value of any independent variable is less than the level of significance, it can be incontrovertibly specified that this parameter can be approved as a significant variable on the dependent variable. The results of the statistical analysis showed that all independent variables had a significant effect on the ultimate axial strength of the CFST and CFDST composite tapered columns since the P-value of each independent variable is less than the significance level value of 0.05. Even though all independent variables are statistically significant parameters on the ultimate axial strength, the degree of effectiveness of each independent variable should also be stated. Therefore, the contributions of the independent variables on the ultimate axial strength of the CFST and CFDST composite tapered columns are given as a percentage in the last column of Table 6. The higher percent contribution of the independent variable implies the higher effectiveness of this variable on the dependent variable.

Table 6 Statistical analysis of the predicted ultimate axial strength of the CFST and CFDST composite tapered columns

| Dependent variable | Independent variable | Sequential sum of squares | Computed F | P-value | Significance | Contribution (%) |
|---|---|---|---|---|---|---|
| $(N_{u,FEM})_{CFST}$ | $\theta$ | 12300125 | 295.16 | 0.000 | YES | 66.1 |
| | $f_{sy}$ | 1642680 | 213.44 | 0.000 | YES | 8.8 |
| | $f_{cu}$ | 4447327 | 157.67 | 0.000 | YES | 23.9 |
| | Error | 229202 | - | - | - | 1.2 |
| | Total | 18619334 | - | - | - | - |
| $(N_{u,FEM})_{CFDST}$ | $\theta$ | 5030803 | 746.12 | 0.000 | YES | 57.3 |
| | $f_{sy}$ | 2125873 | 470.77 | 0.000 | YES | 24.2 |
| | $f_{cu}$ | 1587111 | 1261.15 | 0.000 | YES | 18.1 |
| | Error | 37085 | - | - | - | 0.4 |
| | Total | 8780872 | - | - | - | - |

Table 7 Statistical analysis for the predicted ultimate axial load ($N_{u,FEM}$) of the tapered columns: Effect of tapered angle ($\theta$), steel tube yield strength ($f_{sy}$), concrete strength ($f_{cu}$), and column type

| Dependent variable | Independent variable | Sequential sum of squares | Computed F | P-value | Significance | Contribution (%) |
|---|---|---|---|---|---|---|
| $N_{u,FEM}$ | $\theta$ | 16530489 | 395.33 | 0.000 | YES | 42.8 |
| | $f_{sy}$ | 3753001 | 132.60 | 0.000 | YES | 9.7 |
| | $f_{cu}$ | 5673284 | 100.23 | 0.000 | YES | 14.7 |
| | *Column type* | 11188802 | 146.02 | 0.000 | YES | 29.0 |
| | Error | 1443432 | - | - | - | 3.7 |
| | Total | 38589007 | - | - | - | - |

According to the percent contribution values presented in Table 6, the most important parameter with contribution values of 66.1% and 57.3% that influences the ultimate strength of both CFST and CFDST composite tapered columns is the tapered angle. However, the concrete compressive strength with a contribution value of 23.9% is the second effective parameter on the ultimate axial strength of CFST composite tapered columns whereas the second important parameter that affects the load-carrying capacity of CFDST composite tapered columns is the yield strengths of steel tubes with the contribution value of 24.2%. Moreover, to understand the efficiency of the column type on the ultimate axial strength of composite tapered columns, further statistical analysis was conducted. In this case, in addition to the tapered angle, steel tube(s) yield strength, and concrete compressive strength, the column type was used as another independent variable. Dummy variables were used to identify the column type. In this way, the results tabulated in Table 7 were achieved. It is overtly seen that all independent variables were statistically significant parameters since the P-value of each independent variable is less than the significance level, namely, 0.05. Furthermore, the statistical analysis reveals that the tapered angle with a percent contribution value of 42.8 is the most remarkable parameter on the ultimate axial strength of the composite tapered columns. The second most important independent parameter is the column type with a contribution value of 29.0%. As a result, it can be concluded that the ultimate axial strength of the composite tapered column is directly influenced by the tapered angle and column type.

## 6. Conclusions

With the reference to the aforementioned findings, the following conclusions could be drawn:

- The FEM can be a useful tool for the modeling of the CFST and CFDST composite tapered columns with the circular section. The model proposed by FEM has the veridical ultimate axial strengths, which mean no zero values or no under zero values.
- The results revealed that the proposed FEM model has a good, reliable, and accurate prediction capability. It can be employed in the simulation of both CFST and CFDST composite tapered columns.
- The proposed FEM model can be used in both estimating the ultimate axial strength and indicating the failure mode of the CFST and CFDST composite tapered columns. This can be considered as the unique side of the FEM model developed in the current study.
- Since the tapered columns have a decreasing cross-section with increasing height and the confinement effect provided by the steel tube is directly related to the cross-section, the FEM model is developed taking into consideration the bottom and top cross-sections of tapered columns. The developed FEM model has reliable and meaningful results in both cases.
- The verified FEM model was used to carry out a parametric study in which the influence of the tapered angle and material strength was simulated. It was achieved from the parametric study results that increasing the tapered angle adversely influenced the load-carrying capacity of both CFST and CFDST composite tapered columns.
- In addition, it was observed that the CFST composite tapered columns have higher ultimate axial strength values than the CFDST columns when the samples having the same mechanical and sectional properties are compared.
- Increasing the tapered angle systematically decreased the initial rigidity and displacement value at the peak strength of both CFST and CFDST tapered columns.
- The higher the concrete compressive strength, the steeper descending in the post-peak behavior.
- The steel tube yield strength did not significantly affect the load-displacement behavior of both CFST and CFDST tapered columns, however, remarkably enhanced the load-carrying capacity.
- According to the statistical analysis performed in this study, it was seen that the steel tube yield strength, concrete compressive strength, tapered angle, and column type are statistically meaningful input parameters on the load-carrying capacity. However, regarding the percent contribution in both types of columns, the highest effectiveness degree belongs to the tapered angle.
- Besides, it was noticed that while the yield strengths of steel tubes were the second important parameter influencing the ultimate axial strength of the CFDST composite tapered columns, the ultimate axial strength of CFST columns was more influenced by the concrete compressive strength than the steel tube yield strength.
- In the end, to demonstrate the effectiveness of the column type, further statistical analysis was conducted by using dummy variables. The statistical analysis showed that in addition to the tapered angle, the column type was a significant parameter affecting the load-carrying capacity of the composite tapered columns.

## Declaration of competing interest

The authors declare that they have no known competing financial interests or personal relationships that could have appeared to influence the work reported in this paper.

## Funding statement

This study was not funded by any supporter.

## Data availability statement

All data, models, or code generated or used during the study appear in the submitted article.

## References


American Concrete Institute (ACI 318-08) (2008), Building code requirements for structural concrete, Am. Concr. Inst.

Bažant, Z.P. and Becq-Giraudon, E. (2002), "Statistical prediction of fracture parameters of concrete and implications for choice of testing standard", *Cem. Concr. Res.*, **32**(4), 529-556. https://doi.org/10.1016/S0008-8846(01)00723-2

Binici, B. (2005), "An analytical model for stress-strain behavior of confined concrete", *Eng. Struct.*, **27**(7), 1040-1051. https://doi.org/10.1016/j.engstruct.2005.03.002

CEBFIP (1993), CEB-FIP model code 1990: design code.

Chen, J., Liu, X., Liu, H. and Zeng, L. (2018), "Axial compression behavior of circular recycled concrete-filled steel tubular short columns reinforced by silica fume and steel fiber", *Steel Compos. Struct., Int. J.*, **27**(2), 193-200. https://doi.org/10.12989/scs.2018.27.2.193

D'Aniello, M., Güneyisi, E.M., Landolfo, R. and Mermerdaş, K. (2014), "Predictive models of the flexural overstrength factor for steel thin-walled circular hollow section beams", *Thin-Wall. Struct.*, **94**, 67-78. https://doi.org/10.1016/j.tws.2015.03.020

D'Aniello, M., Güneyisi, E.M., Landolfo, R. and Mermerdaş, K. (2015), "Analytical prediction of available rotation capacity of cold-formed rectangular and square hollow section beams", *Thin-Wall. Struct.*, **77**, 141-152. https://doi.org/10.1016/j.tws.2013.09.015

Ding, F.X., Ding, X.Z., Liu, X.M., Wang, H.B., Yu, Z.W. and Fang, C.J. (2017), "Mechanical behavior of elliptical concrete-filled steel tubular stub columns under axial loading", *Steel Compos. Struct., Int. J.*, **25**(3), 375-388. https://doi.org/10.12989/scs.2017.25.3.375

European Standard (2004), Eurocode 2: Design of concrete structures - Part 1-1: General rules and rules for buildings, Management.

Guo, L., Zhang, S., Kim, W.J. and Ranzi, G. (2007), "Behavior of square hollow steel tubes and steel tubes filled with concrete", *Thin-Wall. Struct.*, **45**(12), 961-973. https://doi.org/10.1016/j.tws.2007.07.009

Han, L.H., Tao, Z., Huang, H. and Zhao, X.L. (2004), "Concrete-filled double skin (SHS outer and CHS inner) steel tubular beam-columns", *Thin-Wall. Struct.*, **42**(9), 1329-1355. https://doi.org/10.1016/j.tws.2004.03.017

Han, L.H., Yao, G.H. and Tao, Z. (2007), "Performance of concrete-filled thin-walled steel tubes under pure torsion", *Thin-Wall. Struct.*, **45**(1), 24-36. https://doi.org/10.1016/j.tws.2007.01.008

Han, L.H., Ren, Q.X. and Li, W. (2010), "Tests on inclined, tapered and STS concrete-filled steel tubular (CFST) stub columns", *J. Constr. Steel Res.*, **66**, 1186-1195. https://doi.org/10.1016/j.jcsr.2010.03.014

Han, L.H., Ren, Q.X. and Li, W. (2011), "Tests on stub stainless steel concrete carbon steel double-skin tubular (DST) columns", *J. Constr. Steel Res.*, **67**, 437-452. https://doi.org/10.1016/j.jcsr.2010.09.010

Hassan, M.M., Mahmoud, A.A. and Serror, M.H. (2016), "Behavior of concrete-filled double skin steel tube beam columns", *Steel Compos. Struct., Int. J.*, **22**(5), 1141-1162. https://doi.org/10.12989/scs.2016.22.5.1141

Hassanein, M.F. and Kharoob, O.F. (2014), "Analysis of circular concrete-filled double skin tubular slender columns with external stainless steel tubes", *Thin-Wall. Struct.*, **79**, 23-37. https://doi.org/10.1016/j.tws.2014.01.008

Hassanein, M.F., Kharoob, O.F. and Liang, Q.Q. (2013), "Circular concrete-filled double skin tubular short columns with external stainless steel tubes under axial compression", *Thin-Wall. Struct.*, **56**, 252-263. https://doi.org/10.1016/j.tws.2013.08.017

Hassanein, M.F., Patel, V.I., El Hadidy, A.M., Al Abadi, H. and Elchalakani, M. (2018), "Structural behavior and design of elliptical high-strength concrete-filled steel tubular short compression members", *Eng. Struct.*, **173**, 495-511. https://doi.org/10.1016/j.engstruct.2018.07.023

Hu, H.T. and Schnobrich, W.C. (1989), "Constitutive modeling of concrete by using nonassociated plasticity", *J. Mater. Civ. Eng.*, **1**(4), 199-216. https://doi.org/10.1061/(ASCE)0899-1561(1989)1:4(199)

Hu, H.T., Huang, C.S., Wu, M.H. and Wu, Y.M. (2003), "Nonlinear Analysis of Axially Loaded Concrete-Filled Tube Columns with Confinement Effect", *J. Struct. Eng.*, **129**(10), 1322-1329. https://doi.org/10.1061/(ASCE)0733-9445(2003)129:10(1322)

Huang, H., Han, L.H., Tao, Z. and Zhao, X.L. (2010), "Analytical behaviour of concrete-filled double skin steel tubular (CFDST) stub columns", *J. Constr. Steel Res.*, **66**, 542-555. https://doi.org/10.1016/j.jcsr.2009.09.014

İpek, S. and Güneyisi, E. (2020), "Nonlinear finite element analysis of double skin composite columns subjected to axial loading", *Arch. Civ. Mech. Eng.*, **20**, 9. https://doi.org/10.1007/s43452-020-0012-x

İpek, S., Erdoğan, A. and Güneyisi, E. (2021), "Compressive behavior of concrete-filled double skin steel tubular short columns with the elliptical hollow section", *J. Build. Eng.*, **38**, 102200. https://doi.org/10.1016/j.jobe.2021.102200

Jamaluddin, N., Lam, D., Dai, X.H. and Ye, J. (2013), "An experimental study on elliptical concrete filled columns under axial compression", *J. Constr. Steel Res.*, **87**, 6-16. https://doi.org/10.1016/j.jcsr.2013.04.002

Kim, J.K., Kwak, H.G. and Kwak, J.H. (2013), "Behavior of hybrid double skin concrete filled circular steel tube columns", *Steel Compos. Struct., Int. J.*, **14**(2), 191-204. https://doi.org/10.12989/scs.2013.14.2.191

Kmiecik, P. and Kamiński, M. (2011), "Modelling of reinforced concrete structures and composite structures with concrete strength degradation taken into consideration", *Arch. Civ. Mech. Eng.*, **11**(3), 623-636. https://doi.org/10.1016/S1644-9665(12)60105-8

Kulak, G.L. (1996), "Tubular members – large and small", *Eng. Struct.*, **18**(10), 745-751. https://doi.org/10.1016/0141-0296(96)00013-2

Lam, D., Dai, X.H., Han, L.H., Ren, Q.X. and Li, W. (2012), "Behaviour of inclined, tapered and STS square CFST stub columns subjected to axial load", *Thin-Wall. Struct.*, **54**, 94-105. https://doi.org/10.1016/j.tws.2012.02.010

Li, W., Ren, Q.X., Han, L.H. and Zhao, X.L. (2012), "Behaviour of tapered concrete-filled double skin steel tubular (CFDST) stub columns", *Thin-Wall. Struct.*, **57**, 37-48. https://doi.org/10.1016/j.tws.2012.03.019

Li, W., Han, L.H., Ren, Q.X. and Zhao, X.L. (2013), "Behavior and calculation of tapered CFDST columns under eccentric compression", *J. Constr. Steel Res.*, **83**, 127-136. http://dx.doi.org/10.1016/j.jcsr.2013.01.010

Lin, M.L. and Tsai, K.C. (2001), "Behaviour of double-skinned composite steel tubular columns subjected to combined axial flexural loads", *Proceedings of the 1st International Conference on Steel and Composite Structures*, Pusan, Korea.

Mander, J.B., Priestley, M.J.N. and Park, R. (1988), "Theoretical Stress-Strain Model for Confined Concrete", *J. Struct. Eng.*, **114**(8), 1804-1826. https://doi.org/10.1061/(ASCE)0733-9445(1988)114:8(1804)

Papanikolaou, V.K. and Kappos, A.J. (2007), "Confinement-sensitive plasticity constitutive model for concrete in triaxial compression", *Int. J. Solids Struct.*, **44**(21), 7021-7048. https://doi.org/10.1016/j.ijsolstr.2007.03.022

Rabbat, B.G. and Russell, H.G. (1985), "Friction Coefficient of Steel on Concrete or Grout", *J. Struct. Eng.*, **111**(3), 505-515.

https://doi.org/10.1061/(ASCE)0733-9445(1985)111:3(505)
Ren, Q.X., Han, L.H., Hou, C. and Hua, Y.X. (2017), "Experimental behaviour of tapered CFST columns under combined compression and bending", *J. Constr. Steel Res.*, **128**, 39-52. https://doi.org/10.1016/j.jcsr.2016.08.005
Richart, F., Brandtzaeg, A. and Brown, R.L. (1928), "A Study of the Failure of Concrete under Combined Compressive Stresses, Bulletin No. 26", Univ. Illinois Bull., Urbana, IL, USA.
Sanez, L.P. (1964), "Discussion of 'Equation for the stress-strain curve of concrete' by Desayi and Krishman", *J. Am. Concr. Inst.*, **61**, 1229-1235.
Schneider, B.S.P. and Member, A. (1998), "Axially loaded concrete-filled steel tubes", *J. Struct. Eng.*, **124**(10), 1125-1138. https://doi.org/10.1061/(ASCE)0733-9445(1998)124:10(1125)
Seow, P.E.C. and Swaddiwudhipong, S. (2005), "Failure Surface for Concrete under Multiaxial Load—a Unified Approach", *J. Mater. Civ. Eng.*, **17**(2), 219-228. https://doi.org/10.1061/(ASCE)0899-1561(2005)17:2(219)
Shekastehband, S., Mohammadbagheri, S. and Taromi, A. (2018), "Seismic behavior of stiffened concrete-filled double-skin tubular columns", *Steel Compos. Struct.*, *Int. J.*, **27**(5), 577-598. https://doi.org/10.12989/scs.2018.27.5.577
Tao, Z., Han, L.H. and Zhao, X.L. (2004), "Behaviour of concrete-filled double skin (CHS inner and CHS outer) steel tubular stub columns and beam-columns", *J. Constr. Steel Res.*, **60**(8), 1129-1158. https://doi.org/10.1016/j.jcsr.2003.11.008
Tao, Z., Wang, X.Q. and Uy, B. (2013a), "Stress-Strain Curves of Structural and Reinforcing Steels after Exposure to Elevated Temperatures", *J. Mater. Civ. Eng.*, **25**(9), 1306-1316. https://doi.org/10.1061/(ASCE)MT.1943-5533.0000676
Tao, Z., Wang, Z.B. and Yu, Q. (2013b), "Finite element modelling of concrete-filled steel stub columns under axial compression", *J. Constr. Steel Res.*, **89**, 121-131. https://doi.org/10.1016/j.jcsr.2013.07.001
Tomii, M., Yoshimura, K. and Morishita, Y. (1977), "Experimental Studies on Concrete-Filled Steel Tubular Stub Columns Under Concentric Loading", *International Colloquium on Stability of Structures Under Static and Dynamic Loads*, Washington, D.C., USA.
Tomlinson, M.J., Tomlinson, A., Chapman, M.L., Jefferson, A.D. and Wright, H.D. (1989), "Shell composite construction for shallow draft immersed tube tunnels", *Proceedings of ICE International Conference on Immersed Tube Tunnel Techniques*.
Uenaka, K., Kitoh, H. and Sonoda, K. (2010), "Concrete filled double skin circular stub columns under compression", *Thin-Wall. Struct.*, **48**(1), 19-24. https://doi.org/10.1016/j.tws.2009.08.001
User, A.S. (2014), "Abaqus 6.14", Dassault Systèmes Simulia Corp., Provid. RI, USA.
Wei, S., Mau, S.T., Vipulanandan, C. and Mantrala, S.K. (1995), "Performance of New Sandwich Tube under Axial Loading: Experiment", *J. Struct. Eng.*, **121**(12), 1806-1814. https://doi.org/10.1061/(ASCE)0733-9445(1995)121:12(1806)
William, K. and Warnke, E. (1975), "Constitutive model for the triaxial behavior of concrete", *Proceedings of International Association for Bridge and Structural Engineering 19*, Bergamo, Italy.
Wright, H.D., Oduyemi, T.O.S. and Evans, H.R. (1991a), "The design of double skin composite elements", *J. Constr. Steel Res.*, **19**, 111-132. https://doi.org/10.1016/0143-974X(91)90037-2
Wright, H.D., Oduyemi, T.O.S. and Evans, H.R. (1991b), "The experimental behaviour of double skin composite elements", *J. Constr. Steel Res.*, **19**, 91-110. https://doi.org/10.1016/0143-974X(91)90036-Z
Xiong, D.X. and Zha, X.X. (2007), "A numerical investigation on the behaviour of concrete-filled steel tubular columns under initial stresses", *J. Constr. Steel Res.*, **63**(5), 599-611. https://doi.org/10.1016/j.jcsr.2006.07.002
Yang, H., Lam, D. and Gardner, L. (2008), "Testing and analysis of concrete-filled elliptical hollow sections", *Eng. Struct.*, **30**, 3771-3781. https://doi.org/10.1016/j.engstruct.2008.07.004
Yu, T., Teng, J.G., Wong, Y.L. and Dong, S.L. (2010), "Finite element modeling of confined concrete-I: Drucker-Prager type plasticity model", *Eng. Struct.*, **32**(3), 665-679. https://doi.org/10.1016/j.engstruct.2009.11.014
Zhang, Y., Fu, G.Y., Yu, C.J., Chen, B., Zhao, S.X. and Li, S.P. (2016), "Experimental behavior of circular fly ash-concrete-filled steel tubular stub columns", *Steel Compos. Struct.*, *Int. J.*, **22**(4), 821-835. https://doi.org/10.12989/scs.2016.22.4.821
Zhao, X.L. and Han, L.H. (2006), "Double skin composite construction", *Prog. Struct. Eng. Mater.*, **8**(3), 93-102. https://doi.org/10.1002/pse.216
Zhao, X.L., Grzebieta, R. and Elchalakani, M. (2002a), "Tests of concrete-filled double skin CHS composite stub columns", *Steel Compos. Struct.*, *Int. J.*, **2**(2), 129-142. https://doi.org/10.12989/scs.2002.2.2.129
Zhao, X.L., Grzebieta, R., Ukur, A. and Elchalakani, M. (2002b), "Tests of concrete-filled double skin (SHS outer and CHS inner) composite stub columns", *Proceedings of the Third International Conference on Advances in Steel Structures*, Hong Kong, China.
Zhao, X.L., Tong, L.W. and Wang, X.Y. (2010), "CFDST stub columns subjected to large deformation axial loading", *Eng. Struct.*, **32**(3), 692-703. https://doi.org/10.1016/j.engstruct.2009.11.015

*CC*